THE UNIVERSITY OF WARWICK

AUTHOR: **Richard Palmer** DEGREE: **MSc**

TITLE: **Characterising the Stellar Population of the NGTS Prototype**

DATE OF DEPOSIT: .....

I agree that this thesis shall be available in accordance with the regulations governing the University of Warwick theses.

I agree that the summary of this thesis may be submitted for publication.

I **agree** that the thesis may be photocopied (single copies for study purposes only).

Theses with no restriction on photocopying will also be made available to the British Library for microfilming. The British Library may supply copies to individuals or libraries. subject to a statement from them that the copy is supplied for non-publishing purposes. All copies supplied by the British Library will carry the following statement:

> "Attention is drawn to the fact that the copyright of this thesis rests with its author. This copy of the thesis has been supplied on the condition that anyone who consults it is understood to recognise that its copyright rests with its author and that no quotation from the thesis and no information derived from it may be published without the author's written consent."

AUTHOR'S SIGNATURE: .....

USER'S DECLARATION

1. I undertake not to quote or make use of any information from this thesis without making acknowledgement to the author.
2. I further undertake to allow no-one else to use this thesis while it is in my care.

DATE SIGNATURE ADDRESS

.....

.....

.....

.....

.....

Characterising the Stellar Population of the NGTS Prototype

by

Richard Palmer

Thesis

Submitted to the University of Warwick

for the degree of

Master of Science

Physics

January 2013

THE UNIVERSITY OF WARWICK

Contents

List of Tables

List of Figures

Acknowledgments

This project relies on NGTS prototype data acquired by James McCormac (PhD 2012, Queens University Belfast)

This research made use of tools provided by Astrometry.net.

This research acknowledges the use of the Carlsberg Meridian Catalogue.

This research acknowledges the use of the PPMXL catalogue.

This research makes use of data products from the Two Micron All Sky Survey, which is a joint project of the University of Massachusetts and the Infrared Processing and Analysis Center/California Institute of Technology, funded by the National Aeronautics and Space Administration and the National Science Foundation.

This research has made use of the SIMBAD database, operated at CDS, Strasbourg, France.

This research has made use of the VizieR catalogue access tool, CDS, Strasbourg, France. The original description of the VizieR service was published in AAS 143, 23.

This thesis was typeset with LaTeX 2_ε[1] by the author.

[1] LaTeX 2_ε is an extension of LaTeX. LaTeX is a collection of macros for TeX. TeX is a trademark of the American Mathematical Society. The style package *warwickthesis* was used.

Declarations

I declare that this thesis is my own, original work except where it has been explicitly stated within the work. In instances of collaborative research my own contribution has been indicated. Use of other published material is clearly acknowledged or referenced. I declare that my own original work has not been published prior to submission of this document and has not been submitted to another University for a degree at any level.

Abstract

Using data acquired by the NGTS Prototype telescope which operated in La Palma during the final months of 2009 and early 2010 I set out to characterise the observed stellar population. I began by astrometrically and photometrically calibrating the images. During the astrometric calibration extensive testing into the speed and accuracy of three astrometric calibration tools was undertaken with the intent of determining their advantages and disadvantages for inclusion in the final NGTS pipeline. The fields studied were searched for variable objects and time series analysis was carried out on one good quality variable. In keeping with the NGTS projects aim to find exoplanets the WASP11 transit was recovered from the data, which also demonstrates the accuracy achieved with the prototype and is promising for the final instrument. A study of the stellar population, focused on M-dwarfs, was undertaken. It was found that the limiting magnitude of the telescope resulted in only a small M-dwarf population being observed, with none of them displaying identifiable variability. The dominant population observed within the analysed fields are K-dwarfs.

Chapter 1

Introduction

Throughout human history we have been able to look at the sky and see that it is never static. The changing positions of our Sun and Moon have dictated our seasons and harvests. The night sky is just as changing, stars wheeling overhead and those planets nearest to us appearing and disappearing from our skies. More infrequent visitors to our skies, comets, have often been seen as bad omens foretelling the death of kings or other important figures. As our ability to look further into the sky has advanced we have seen that there is change and motion everywhere. Moons are seen to orbit the other planets in our solar system prompting an adjustment in our thinking as to our place in the Universe. On a universal scale objects are observed to be receding from each other as the very fabric of the Universe expands, the study of which led to the Big Bang Theory of the Universes beginning.

Whilst motion is the most obvious change in the night sky it is not the only one. Stars get brighter or dimmer as objects pass in front of them or they explode. These stars in particular are of great interest to us as they can tell us much about the Universe. Eclipsing binary systems for example provide the only opportunity for stellar masses and radii to be determined. Planetary transits across a star are a powerful means of detecting extra solar planets and can provide us with important clues about said planets. The answer to the questions of whether there are other Earth-like worlds out there and whether we are alone in the Universe can be advanced here.

To obtain these answers we must first study the objects in our sky to then analyse what we see and understand how they change. In my project I took the data acquired by the NGTS prototype telescope (Chapt. 2) and carried out a study of the stellar population contained within that data. My main interest in the data was stellar variability and planetary transits (Chapt. 4) but I also looked

at the overall stellar population (Chapt. 5). Knowing accurate sky coordinates of the detected objects and ensuring that the images have good photometry is an important requirement for undertaking this sort of study and so significant time was spent on calibrating the images that I used (Chapt. 3).

1.1 Causes of Variability

There are a variety of causes for stellar variability: flares, an orbiting companion that leads to periodic eclipses, an orbiting planet transiting across the star and stellar pulsations. Figure 1.1 provides examples of what the light curve could look like for several types of variables. From top left to bottom right the figure shows Cepheid variable (an example of stellar pulsations), a recurrent nova, an eclipsing binary and a transiting hot Neptune exoplanet. The morphology of these light curves can vary depending on the stars involved, for example their brightness, sizes and in the case of the binary the distance between them. Even the inclination angle we view the system at can have an impact on the shape of the light curve. Exoplanet searches which seek variable objects as transits are a key means of detecting said planets. Currently most transiting planets detected are larger than our own Earth due to the fact that a larger planet blocks out more light and therefore causes a more detectable reduction in the observed magnitude of the star. We can distinguish the exoplanet transit from the eclipsing binary in Figure 1.1 by the fact that a planet is much smaller than the host star leading to a smaller variation in magnitude whilst it passes in front of the host star. However false positives can occur in the case where the system being observed is an eclipsing binary viewed at an angle that reduced the depth of the eclipse to planet like proportions, or the light of a foreground star is diluted by a fainter background eclipsing binary. The only way to eliminate these is in depth analysis using large telescopes and spectroscopy.

The formal description of a transit is that the entire body of the eclipsing body passes in front of the star. Our observation of this depends on the angle at which we view the system. To catch a transit it is necessary to view a system edge on, or nearly so, and therefore transiting planets are only a small sub sample of the exoplanets in the observable Universe.

Observations of transits allows us to determine many facts about the planet, with mass and radius being the main interest. Study of the transit light curve can give a star to planet radius ratio. This ratio is frequently determined and has its own symbol k and a simple formulation is available in equation 1.1, where $R_\star$ is the radius of the star, R_p is the planet radius and δ is the transit depth. Using the radial

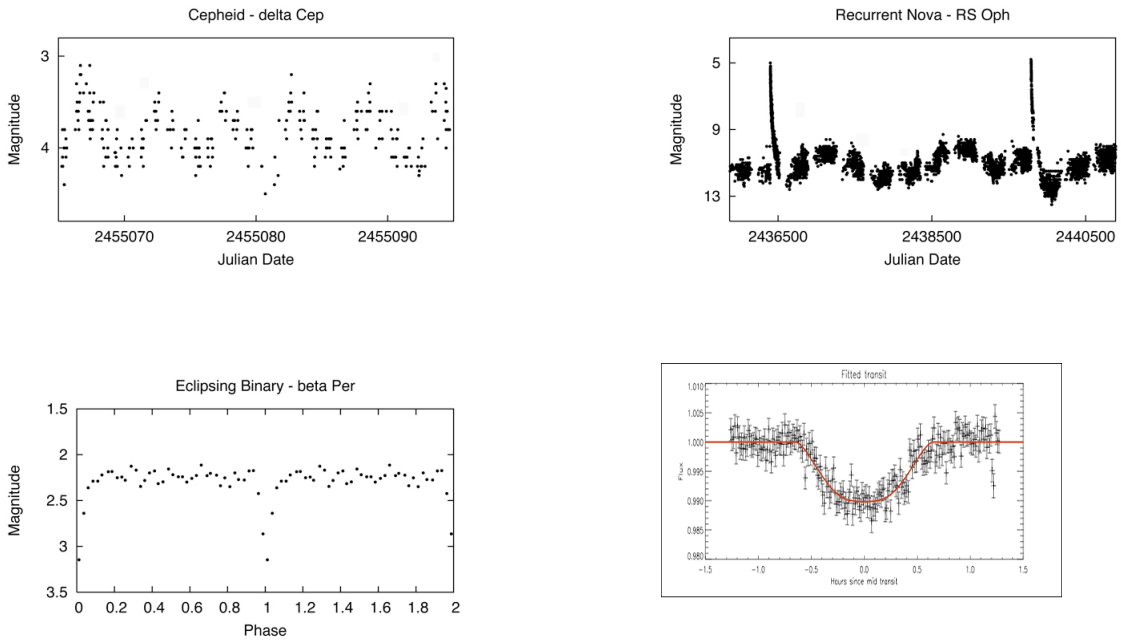

Figure 1.1: Four light curves showing examples of variability. From top left to bottom right, a Cepheid variable, a recurrent nova, an eclipsing binary, all from AAVSO [AAVSO, 2011], and a transiting planet viewed by the NGTS prototype [NGTS Partner Institutes, 2012].

velocity of the star and its mass, obtained using stellar models through observation of its spectral class the minimum mass for the planet can be determined.

$$k \equiv \left(\frac{R_p}{R_\star}\right) \approx \sqrt{\delta} \tag{1.1}$$

$$\left(\frac{M_p}{(M_p + M_\star)^{2/3}}\right) = \left(\frac{K_\star\sqrt{1-e^2}}{\sin(i)}\right)\left(\frac{P}{2\pi G}\right)^{1/3} \tag{1.2}$$

Equation 1.2 provides a formulation for determining the minimum planet mass. M_p is the planet mass, $M_\star$ is the star mass, $K_\star$ is the velocity semiamplitude, i is the inclination, P the period and G the gravitational constant. Observing a transit means $\sin(i) \approx 1$ and observations of multiple transits over an extended period of time gives the period. However the data usually only allows a determination of $\left(\frac{M_p}{(M_\star)^{2/3}}\right)$ and not M_p.

Observations of successive transits allows the determination of the orbital period of the body. Determination of this makes it possible to calculate the separation between the star and the planet by using Kepler's third law, a generalised version of which is given in Equation 1.3, P being the period and R the radius. These observations also give the occulation depth, δ_{occ}, the small reduction in brightness by the star obscuring the planet and losing the light reflected by the planet. It is possible to calculate the planets thermal emission using this. Assuming the planet dominates emissions at long wavelength and approximating planet and star to black bodies we get Equation 1.4 in which $B_\lambda(T)$ is the Planck function, Equation 1.5. It is also possible to carry out transmission spectroscopy on the planets atmosphere along the assumption that some of the light will be passing through the atmosphere of the planet during the transit. This makes it possible to suggest what the composition of the planets atmosphere could be like [Winn, 2011].

$$\frac{4\pi^2}{P^2} = \frac{GM}{R^3} \tag{1.3}$$

$$\delta_{occ}(\lambda) = k^2\left(\frac{B_\lambda(T_p)}{B_\lambda(T_\star)}\right) \rightarrow k^2\left(\frac{T_p}{T_\star}\right) \tag{1.4}$$

$$B_\lambda(T) \equiv \left(\frac{2hc^2}{\lambda^5}\right)\left(\frac{1}{e^{\frac{hc}{(\lambda)k_BT}} - 1}\right) \rightarrow \left(\frac{2k_BT}{\lambda^2}\right) \tag{1.5}$$

1.2 Previous Surveys

1.2.1 Near Earth Objects

The study of variability in the night sky is a major area of astronomy and many projects have been devoted to studying the various types of variability. From surveys looking at supernovae with the intent of determining their progenitors, especially for those of type Ia to those seeking planets around other stars. Closer to home we have the search for the many asteroids in our local system to determine where they are, where they might go and discover what they can tell us about the early solar system. On this local scale the Catalina Sky Survey is aiming to build an inventory of near Earth Objects of particular hazardous asteroids, those that pose an impact risk to our world. The survey consists of three separate sub-surveys the (original) Catalina Sky Survey, the Mt. Lemmon Survey and Siding Spring Survey. The Mt. Lemmon Survey is also used to provide characterisation of the objects particularly size, density and velocity, all key requirements to assess the threat the objects pose [Hill, 2003].

The Catalina Sky Survey is not alone in seeking hazardous objects, Pan Starrs also undertakes searches for near Earth objects and the wide field nature of its repetitive observations also makes it suitable for observations of objects beyond our solar system. In particular by being able to map large areas of the sky to great sensitivity it can seek variable objects of all types. It has the ability and potential to find e.g. exoplanets, observe white dwarfs and neutron stars with companions and study young stellar objects [Institute for Astronomy University of Hawaii, 2005].

Pan Starrs has the capability to study the more explosive elements of our Universe. Candidates for Type Ia supernovae can be determined and light curves generated, though follow up observations are required for proper analysis. It has the ability to detect the afterglows of gamma ray bursts, providing a statistical basis for determining the astrophysical environments that cause them. Finally, through variability monitoring it can detect active galactic nuclei [Institute for Astronomy University of Hawaii, 2005].

1.2.2 Short Time Scale Variability Surveys

Of particular relevance to my project are those surveys that have dealt with short time-scale variability, faint objects and planetary transits. The RApid Temporal Survey (RATS) searched for short time scale variability. Short time scale variability is important, as it is thought to occur in systems consisting of close white dwarf pairs, and these are of interest to several future projects such as gravitational wave

radiation experiments. Theoretical models predicted the existence of more of these systems then had been identified observationally. The RApid Temporal Survey project was set up to help resolve this problem and, as a by product, was likely to discover many other short time-scale variable systems.

Using the Isaac Newton Telescope (INT) and the Wide Field Camera (WFC) RATS observed 12 fields covering 3 square degrees. It was sensitive to variations on timescales as short as two minutes and could achieve a magnitude depth in V$\simeq$ 22.5. The survey discovered 45 objects with significant short term variability with four systems showing variations on timescales of less than an hour, and the shortest varying on a time scale of 374 seconds [Ramsay and Hakala, 2005]. The survey had additional follow up photometry and spectroscopy to gain a full understanding of the short period variables, with the results published in Ramsay et al. [2006].

While RATS was not the first survey to seek variations below timescales of a day it was definitely the most important project to search on very short timescales. However, it covered a very small area of the sky and was certainly not the deepest magnitude wise. Different surveys offer different views based on the observations taken. The same telescope and camera that carried out RATS were used by the Faint Sky Variability Survey (FSVS) in its search for astrometric or photometrically variable objects on a wide timescale range and with a dynamical range of 16 to 24. It also covered a larger area of the sky compared to the RApid Temporal Survey, 23 square degrees compared to 3 square degrees initially surveyed by RATS. [Groot et al., 2003]

Within the scope of the survey there was a study of short timescale variability focusing on timescales of 24 minutes to tens of days. Of interest is the finding that about one percent of point sources down to V=24 are variable. The survey also acquired enough data to explore the fraction of variable sources for different spectral types and this is something worth comparing with my project. FSVS discovered that for much of the main sequence the distribution of variables was consistent with one percent being variable. Towards the blue end of the main sequence sequence, F0 to F5 the fraction increased to two percent and for bluer sources above the main sequence, it climbed to 3.5 percent. [Morales-Rueda et al., 2006]

1.2.3 Exoplanet Surveys

Many early exoplanet searches using transits reported disappointing results. This was primarily attributed to the lack of success in acquiring accurate photometry for solar and late main sequence stars. The Wide Angle Search for Planets (WASP) and the SuperWASP cameras are a wide field imaging system capable of giving very

good photometry on bright objects. This separates it from other surveys such as RATS and FSVS, both of which could go to a much greater magnitude depth but could only cover very small areas. WASP could achieve accuracies of better than 1 percent for V of 7 to 11.5 with secure detections as faint as 15th magnitude. It also has the ability to survey very large areas of the sky, each instrument[1] having an angular view of 482 square degrees with a scale of 13.7 arcseconds per pixel. Though normally operating at high cadence it could survey the entire sky in 40 minutes. Its main aim was to search for bright transiting exoplanets that would be suitable for follow up spectrometry. In the first six months the northern telescope acquired data to produce light curves for about 6.7 million objects [Pollacco et al., 2006].

The data reduction pipeline used the USNO-B1.0 catalog for photometric input. Calibration frames were acquired at dusk and dawn on the observing nights. The images required precise astrometry which was achieved through a series of calibration steps. An initial position for the image center could be determined to a few arc minutes using data from the mount position and the known offsets of the cameras. From this a plate solution would then be attempted by searching for patterns using the hundred brightest objects against a reference catalog. From the plate solution a photometric input catalog is created for aperture photometry. Additional post pipeline calibration is carried out [Pollacco et al., 2006].

Transiting exoplanets were not the only thing to be found by WASP. Large numbers of variable stars were also discovered. One subset of interest were ROSAT X-ray sources as they provided an excellent test of WASP's ability to detect other variables that were not transiting exoplanets. A wide range of previously known objects were found that helped to demonstrate the accuracy of the calibration and the ability to determine periods from the data acquired. [Norton et al., 2007]

Short period eclipsing binaries are another subset that were easily detected with WASP and many were new. Purpose written code was used to search for these objects in the WASP data. The period search method used meant that contact binaries would give a period of half the orbital period and this is something to bear in mind when carrying out period searches on the prototype data during my project [Norton et al., 2011].

As of January 2012 the SuperWASP archive contained 1849 nights of data consisting of more than 10 million individual images. More than 30 million unique stars are contained in these images and the discovery of 75 transiting exoplanets had been announced by the project [Norton, 2012].

[1]WASP has two telescopes, one to cover the northern sky placed at Observatorio del Roque de los Muchachos on the island of La Palma in the Canary Islands, and another to cover the southern sky placed at the Sutherland Station of the South African Astronomical Observatory

All ground based surveys are disadvantaged by having to observe through the Earth's atmosphere. This causes many issues and places limits on how accurate the acquired photometry can be. A telescope in space does not suffer from this issue. The Kepler Space Telescope is the front runner for exoplanet surveys. Seeking planets with an orbital period of up to two years it aims to improve our knowledge of the distribution and numbers of exoplanets in or near the habitable zones of stars [NASA, 2012].

However, being space-based it has certain limits, chiefly bandwidth. It can only transfer so much data down in a given time and it is hence limited in the number of stars it can observe. This means that all Kepler observations will be targeted, rather than full field surveys, and it will miss many interesting variable objects.

As its name implies the Next Generation Transit Survey is the next big planet based survey to look for transits. Whilst not going to the same depth as the Faint Sky Variability Survey, it will go to cadences as short, or even shorter, than the RApid Temporal Survey. It also intends to study a very large area of the sky for transits, and as a by product other variability. The project is a collaboration between Queens University Belfast, University of Warwick, University of Leicester, Observatoire de Genève, DLR, Berlin and Universidad Catolica de Chile, some of whom were involved with the WASP surveys and bring the lessons learned and the experience acquired to the NGTS project.

The NGTS survey will search for Neptune-sized and smaller planets around bright stars. It will operate in the 600 to 900nm range which will maximize its sensitivity to K and early M type stars. The site selected for the telescope, Paranal, was influenced by the fact that the observation band can be significantly affected by water, causing poor photometry. The requirement for very good photometry and clear observing nights led to the selection of this excellent observing site [NGTS Partner Institutes, 2012].

Chapter 2

The NGTS Prototype

From October 2009 to July 2010 a prototype of the NGTS telescope took observations intended to test the operation and potential observing parameters for the final project. The prototype consisted of two cameras, but only one of which was functional on a mount of limited traverse. The limited traverse required the telescope to be rotated when the observed field crossed the meridian. This results in a meridian flip halfway through the night. The prototype also lacked an auto-guider, though one will be installed on the final telescope.

The observations were used to test a wide variety of operating parameters, such as exposure times and focusing. The band pass of the filter used on the telescope was 650-950nm. Exposure times range from 30 seconds to 300 seconds, with the majority of the nights using 30 to 60 seconds. Figure 2.1 is an image of the prototype set up on La Palma and Table 2.1 contains some basic data on the equipment[NGTS Partner Institutes, 2012]

The prototype images are around 5.3 arcseconds per pixel in scale with the images having a size of about 1.5 degrees by 1.5 degrees. Exposure times are dependent on the night of observation and are contained in the FITS header along with the approximate coordinates of the field centre and time data. All the image headers follow the FITS standard, however, there is no standardization in content between the data sets.

All the images that I analysed had been dark, bias and flat field calibrated. They had also been divided into the meridians for each night. The image files are identified by the time of observation with additional extensions indicating the calibrations carried out.

The focuses of the following chapters, image calibration (3), a search for stellar variability (4), and characterisation of the stellar population observed by the

Figure 2.1: The NGTS prototype telescope set up on La Palma[NGTS Partner Institutes, 2012].

	Details
CCD	1k×1k e2v
Telescope	8 inch Takahashi
Cameras	2 (Only one functional)
Optimal sensitivity	600-900nm
Active	Winter 2009-2010

Table 2.1: Basic data for the NGTS prototype telescope[NGTS Partner Institutes, 2012].

prototype (5), each have their own requirements that influenced the choices for what data sets to use. Calibration would need to be tested on both extremes of the focus range. This requires a minimum of one data set designated as focused and one designated as defocused. Chapters 4 and 5 both need observations in a 'good' focus and observations on the same field over multiple nights. Also the hope of detecting a planetary transit in Chapter 4 required a night including a known transit.

The night 7th October 2009 was observed as a "focused" night. The majority of the work with this night used the East meridian data set consisting of 515 images with thirty second exposure times. The astrometric calibration in Chapter 3 demonstrated that the meridians for before (East) and after (West) the flip did not line up. This night is suitable for testing calibration techniques for focused images. A minimum of four thousand sources are identified in these observations using source extraction tools.

The night dated 4th February 2010 was observed as a "defocused" night, and contains the WASP 11 transit. This allows the images to be used for both Chapters 3, as a test for the calibration tools on defocused images, and in Chapter 4 as a transit example. Exposure times for these images are 40 seconds, and there are around three thousand sources extracted from the raw images. The early images for the night are of relatively poor quality, with indications of slight cloud and a couple of images being saturated. The available data is limited to a single meridian of observation.

Field 1, as identified in the observing logs, has been observed on many nights with different exposure times. The aim had been to get 3 nights of data for each exposure time at the good focus setting for the telescope. A couple of nights of preliminary exposures also exist but will not be used. The key nights will be the 19th, 21st and 29th November 2009. The separations exist due to nights of bad weather stopping the telescope from operating. These nights are at 30 second exposure times.

At the time of the year, mid to late December, when the 60 second exposures were taken of field 1 the moon was impacting the observations. Therefore several

Night/Field	Date	Target Star	Exposure Time (s)	Shorthand	No. Images
Focused	07/10/2009	SAO 36763	30	20091007	1025
Defocused	04/02/2010	GSC 2340:1714	40	20100204	320
Field 1	19/11/2009 21/11/2009 29/11/2009	SAO 41039	30	20091119 20091121 20091129	718 900 582
Field 1	09/12/2009	SAO 41039	60	20091209	468

Table 2.2: Basic data for selected image sets used in Chapters 3, 4 and 5. All barring 20100204 have data from two meridians and image number corresponds to the complete set for the night.

sub fields were observed and only one of the three nights was actually observing field 1.

Exposure times beyond 60 seconds for field 1 were found to be saturated. This saturation was significant enough to severely impact overall image quality and as such the data sets with longer exposures, 120 and 300 seconds, were not used.

In the end I decided that only four nights for field 1 were of usable quality for my analysis. Three of these nights are at 30 second exposures and one night at 60 seconds. The 21st October night had some potential for poorer quality due to the telescope being forced to shut twice during the night. Table 2.1 contains basic data for the primary data sets to be used in the following chapters.

Chapter 3

Image Calibration

The purpose of this study was to characterise the stellar population of the NGTS prototype images. The images needed to be astrometrically and photometrically calibrated before any analysis could be undertaken. Astrometric calibration converts pixel coordinates to sky coordinates and photometric calibration converts instrumental magnitudes to apparent magnitudes. As the method used for the photometric calibration relied on catalogue information for the extracted objects, it was required that astrometric calibration was carried out first.

3.1 World Coordinate System

The raw images are a 1024 by 1024 pixel grid with a value of the recorded counts for each pixel. To match the objects in an image with a catalogue it is necessary to assign sky coordinates to this pixel grid. The World Coordinate System or WCS information is a standardized way of describing the sky coordinates of an image. The FITS header keywords and the method of determining the relationship between image and sky coordinates for WCS data are laid out in a series of papers detailed below.

The definition involves determining the sky coordinates for a specific point in the image, often the centre though not necessarily, and then giving the relationship between the image pixel increments and sky coordinate increment. With a reference point and the relationship between the increments it is then possible to compute sky coordinates for every pixel in an image. The first paper in the series lays out a generalized example of how this can be achieved, along with the basic FITS header keywords. The basic formalisation is a linear transformation applied via matrix multiplication of the vector of pixel coordinate elements [Greisen and Calabretta,

2002].

$$q_i = \sum_{j=1}^{N} m_{ij}(p_j - r_j) \tag{3.1}$$

In Equation 3.1 p_j is the vector of pixel coordinates, r_j are the pixel coordinates of the reference point and m_{ij} is a non singular square matrix of dimensions $N \times N$. The result, q_i is an intermediate pixel coordinate vector in dimensionless units that describes the offsets from the reference point along axis coincident with the intermediate world coordinates [Greisen and Calabretta, 2002]. This offers an easy conversion to intermediate world coordinate elements, x_i as in Equation 3.2. The axis type, linear or non-linear[1], determines the next step and is covered in the paper.

$$x_i = s_i q_i \tag{3.2}$$

The second paper [Calabretta and Greisen, 2002] in the series investigates in greater depth the implementation of celestial coordinates and spherical map projections which are of greater interest to astronomy. An initial draft of the paper, available as a preprint, contained proposed keywords and definitions for handling image distortions, which was removed from the final published version. This early implementation of the keywords was incorporated into the AstrOmatic[2] software suite, which includes the astrometric calibration code SCAMP that I tested as part of my project. The proposed standard for distortions has been moved to paper four in the sequence, complete with a new set of header keywords. This means that the method used by SCAMP to define distortion will not follow the ultimately adopted version, and is likely incompatible with any tools which use the standard implementation.

Paper three [Greisen et al., 2006] in the series deals with spectroscopy and is not relevant to my project. The fourth paper, as has been mentioned, deals with distortions. However it is still in draft and has been for some time. The lack of a genuine standard for the implementation of distortions in WCS information has become an issue with projects that require a description of distortion within their images, for example the Spitzer Space Telescope. The Spitzer images were all distorted by a few percent and so the Spitzer Science Center developed their own method to describe the distortion in the FITS headers. This method is described

[1] Non-linear axis types are encoded in the FITS header using eight characters in a "4-3" algorithm code, for example TAN–SIP.

[2] www.astromatic.net

as the Simple Imaging Polynomial (SIP) [Shupe et al., 2005] and has become implemented in several other software packages, including Astrometry.net[3] which was used during my project.

The issue that arises with SIP is that though the keyword convention is compliant with the first two papers laying out WCS, and has been influenced by the proposed implementation of distortions in paper four, the keywords are not the same as those proposed. Due to the fact that SIP has become fairly widely used this poses a possible compatibility issues in the future.

3.2 Astrometric Calibration

3.2.1 Tools

The main contribution of the research described here to the overall NGTS project is a study of the various astrometric calibration tools available. In the process of calibrating the images for the search for variable objects, (Chapt. 4) and the study of the observed populations spectral types, (Chapt. 5) I will determine the usefulness and accuracy of the tools that are available. The NGTS project ideally requires an astrometric calibration tool that is both fast, as short exposure times will be used, as well as accurate, able to calibrate to the true position with the smallest error, and precise, able to repeat the accuracy of calibration over many images. Therefore the speed, accuracy and precision of the tools will be of considerable interest when investigating their performance. Ideally the tools will be self contained and require minimal support.

SExtractor

Though not an astrometric calibration tool, SExtractor [Bertin and Arnouts, 1996], a source extraction tool from the AstrOmatic[4] software suite, was used heavily throughout the project. The operation of this tool is controlled through a configuration file and a parameter file provides considerable customization of the output. The output can consist of source parameters such as flux, magnitude data, object position by pixel or sky coordinate[5] and various error flags. The error flags indicate if the extracted source was acquired cleanly, or suffers from de-blending, saturation or bad pixels.

[3] www.astrometry.net
[4] www.astromatic.net
[5] If WCS information exists for the image.

The output file can be a simple ascii table making follow up work on the extracted sources very user friendly. It can also be in several more specialised formats, such as FITS-LDAC, which was a requirement for the input file to the SCAMP astrometric calibration tool. The flux values and magnitudes are extracted without knowledge of the exposure times. The zero point of the values was determined using a calculated reference magnitude for a forty second exposure on the instrument.

WCS Tools

Three astrometric calibration tools were tested. The first of these is part of the WCS Tools[6] [Mink, 2005] software suite. This is a self contained C code package that offers a variety of tools for interacting with the WCS information contained within a FITS image header. This package offers far more than just astrometic calibration and can be used to edit the headers and do basic image manipulation. It also contains a routine for comparing positions given by an image WCS Header compared to catalogue positions, and can generate reference images from catalogues. This was employed extensively throughout the project to determine accuracy of the calibrations.

The main interest though was the astrometric calibration routine. This worked by comparing object image positions to a catalogue to determine an astrometric calibration. The reference catalogue that was chosen was the 2 Micron All Sky Survey or 2MASS catalogue [Skrutskie et al., 2006]. Both the image and a list of source extracted objects must be input to the tool. The source list consists of x and y positions on the pixel grid and the magnitude and *must* be sorted in descending order of brightness to avoid errors.

The source list is matched to a user defined number of reference stars, usually fifty, in the catalogue data of the area of the sky covered by the image. A solution is determined based on the number of matches between the list and reference stars. More matches should provide a better solution and this was seen to hold. From this an astrometric solution is then generated. Additional steps can be specified by the user in an attempt to improve the calibration. These steps are running another calibration using the initial solution as a new image center, additional iterations of the calibration, sigma clipping the worst of the outliers and fitting a quadratic polynomial to improve residuals.

[6] tdc-www.harvard.edu.wcstools

Astrometry.net

A second software package is available from the Astrometry.net[7] site and goes by the same name. Astrometry.net works as black box that, at the basic level takes any image and derives an astrometric solution. This makes it very useful for dealing with corrupt, incorrect or missing WCS header information. If WCS information exists it will attempt to verify this before doing anything else. Regardless of its incorporation in the calibration pipeline for the NGTS project it, will be very useful for dealing with problematic images. The tool works by comparing stars in the images to stars in a set of index files provided with it derived from two catalogues, (USNO-B 1.0 and TYCHO-2 Lang et al. [2010]). These index catalogues are provided upon request from Astrometry.net.

The indexes contain quads of stars. A stars position in the quad is determined by the separation of the stars in the quad meaning the quads are immune to various distortions that can occur in images. The stars in the input images are redefined as quads and then these quads are compared to quads in the indexes that are assembled at the same image scales. Matching the quads will then allow the program to determine an astrometric solution. No additional programs are necessary as it comes with a built in source extractor.

The user can provide a small number of command line parameters that can impact the speed of the search. Providing an initial position means that less of the sky is searched over to begin with, but the program will extend to further areas if no solution occurs. More useful is providing an image scale as this reduces the number of indexes searched, speeding up the process. This is the case because the indexes are based on a certain quad size so many indexes contain quads too big or too small for the images being used. The program searches the indexes with groups of stars and if no solution is found with a group, the number of stars used increases. This increases the search time in each index and there is a hard cut-off of five minutes at which point it will return no solution. This cut-off can be changed in the input commands. It was found, though, that it was very unlikely to reach this cut-off and a solution was usually found within ten to twenty seconds.

SCAMP

The third tool studied extensively in this project was SCAMP [Bertin, 2006], which is part of the AstrOmatic software suite, along with SExtractor described above. Like SExtractor, the user can control many of the functions using a configuration file. The

[7] www.astrometry.net

	20091007	20100204
Date	07/10/2009	04/02/2010
Time	23:38:52	22:29:05
Exposure Time (s)	30	40
JD	2455112.44365741	2455232.43640046
Commanded RA	00:55:42.87	03:10:59.29
Commanded DEC	+48:43:21.57	+29:43:24.90

Table 3.1: Basic image data for the focused (20091007) and defocused (20100204) test images.

input is a specially prepared SExtractor file which is then compared to a catalogue to determine a solution. The catalogue, along with its location, are chosen in the configuration file and for this project the 2MASS catalogue was used. Provided additional code libraries are available SCAMP is capable of outputting plots, which provide additional supporting data, such as distortion, for the calibration.

The tool has issues in that installation requires a large number of additional libraries. More pressing was the fact that SCAMP is not able to operate on the raw images that would be the starting point in this project. The program needs to know an initial relationship between image and sky coordinates provided by a first approximate WCS solution. This reduced SCAMP to being used to improve calibrations done by either WCS Tools or Astrometry.net. Another problem was that it did not write the solution to the image header but to a separate ascii file instead, which is inconvenient when large numbers of images are being solved simultaneously. It is however simple to produce a piece of code that can use the ascii file to update the image headers with the correct keyword values.

3.2.2 Single Image Testing

To test how the tools perform and estimate the speed of operation all tools were tested on a single image to begin with. A focused image from 7th October 2009 and a defocused image from February 4th 2010 were selected. The images are near to the midpoint of the observing sequence for each set. Data for these test images is in Table 3.1. Once a solution had been obtained for the astrometry, the solution was checked for accuracy using a tool from the WCS Tools software suite, "immatch". To use this tool a source list is generated from a catalogue using WCS information in the image, to determine the region of sky and convert the catalogue right ascension and declination to image coordinates. The image and the catalogue data are provided to the tool which then matches objects between them.

This comparison produced a file containing the deviations of the coordinate of all the objects in the image from their catalogue positions and was used to determine the accuracy of the astrometric calibrations of the three packages. Scatter plots of the x and y components of the deviations, the deviations being converted back to pixel units, would show the level of accuracy as an overall units impression. In terms of the image to sky relation, x is right ascension and y is declination. Using Figure 3.1 as an example, a tight circular cluster centred on (0,0) would be an accurate calibration, whilst a more dispersed plot is a poor calibration. A more quantitative determination of the accuracy is achieved by taking Gaussian cross sections of the plots in each axis. Calculating the Full Width Half Maximum (FWHM) of the Gaussian allows the accuracy of the calibration to be quoted numerically.[8]

Astrometry.net

Astrometry.net was the first tool to be successfully employed demonstrating its robustness and ease of use. Providing the image scale cut the number of indexes searched through to three and cut the solve time down to between five and eight seconds, depending on the number of sources in an image. The number of sources was related to the focus, focused being the slower end of the range with up to 5000 sources and defocused at the quicker end with about 3500 sources. Figure 3.1 shows the scatter plots for both calibrations for the images in Table 3.1. The calibration for the defocused image is worse, as expected, given the objects are smeared out over more pixels, resulting in a less accurate determination of the object centre. This is indicated by the FWHMs for the Gaussian cross sections in Figure 3.2 and Figure 3.3.

Both scatter and Gaussian plot indicate a puzzling offset in the y axis the cause of which could not be identified. It would imply that the calibration was out of position in one direction. This could be an indication of distortion along that axis of the image but a robust explanation was never determined. Objects with larger scatter are likely to be those near the edges of the image and therefore be suffering more from distortion. Figure 3.4 shows the total value of the positional offset for the sources as a function of their magnitude. The largest offsets occur at faint magnitudes which is understandable given the faintness of the sources making determining the actual position difficult. The larger offsets for objects at brighter magnitudes can be attributed to the increasing saturation at the bright end of the magnitude range again obscuring the actual object positions.

[8] All Gaussian plots are confined to an axis scale of ± 2 pixels.

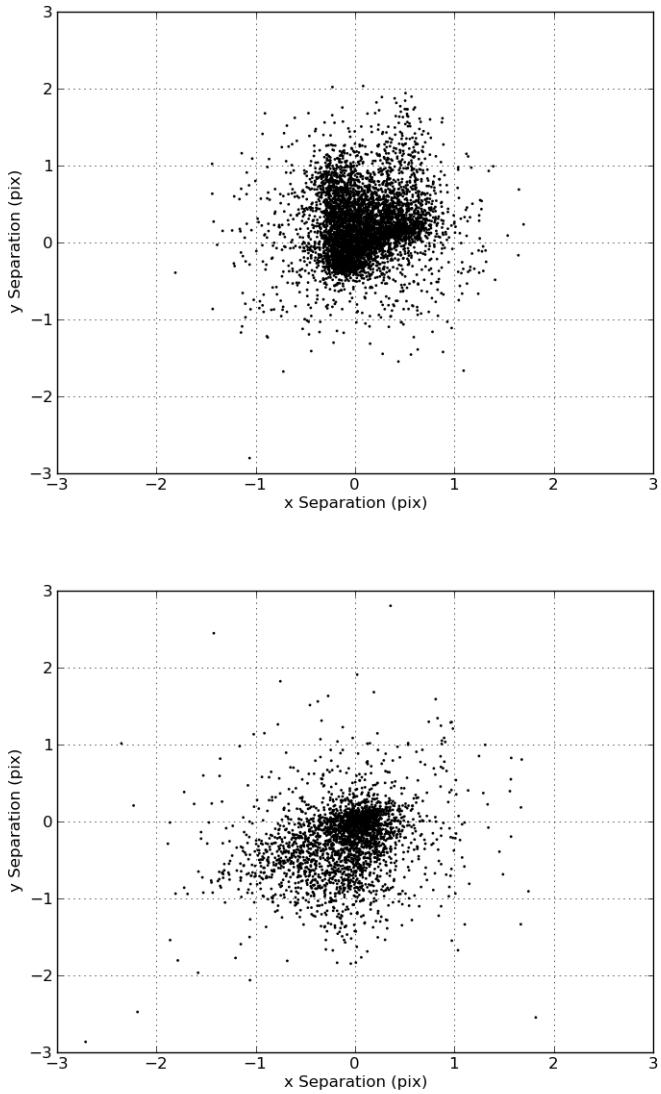

Figure 3.1: Focused and defocused coordinate offsets from Astrometry.net. The image data is in Table 3.1. The top plot is for the focused night and the bottom the defocused night. Both plots have been limited to ±3 pixels and a few outlier points are not shown.

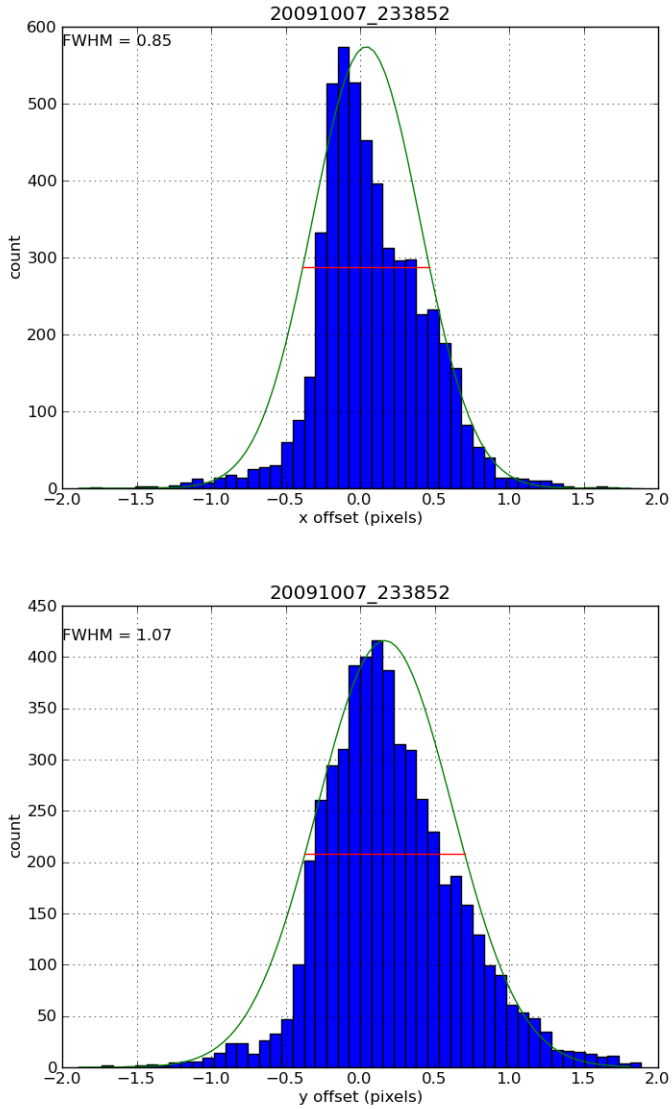

Figure 3.2: Gaussian fits to the cross sections of the top scatter plot (focused) (Astrometry.net calibration) in Figure 3.1. The FWHM of the fits are included on the plots. The Gaussian overlays indicate an offset to the calibration.

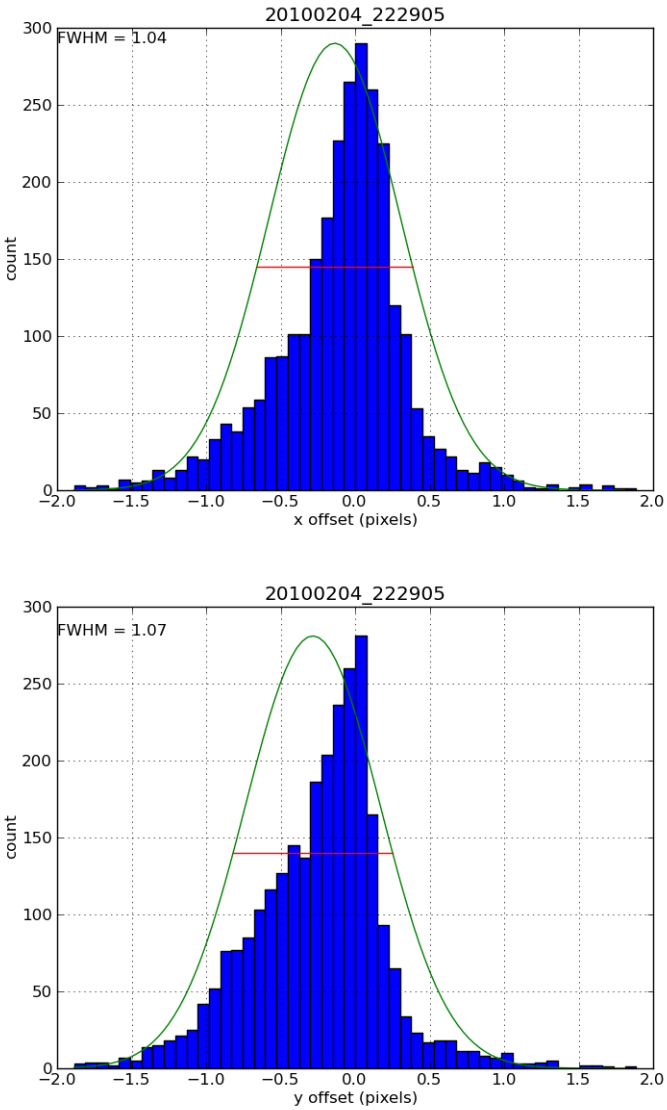

Figure 3.3: Gaussian fits to the cross sections of the bottom scatter plot (defocused) (Astrometry.net calibration) in Figure 3.1.

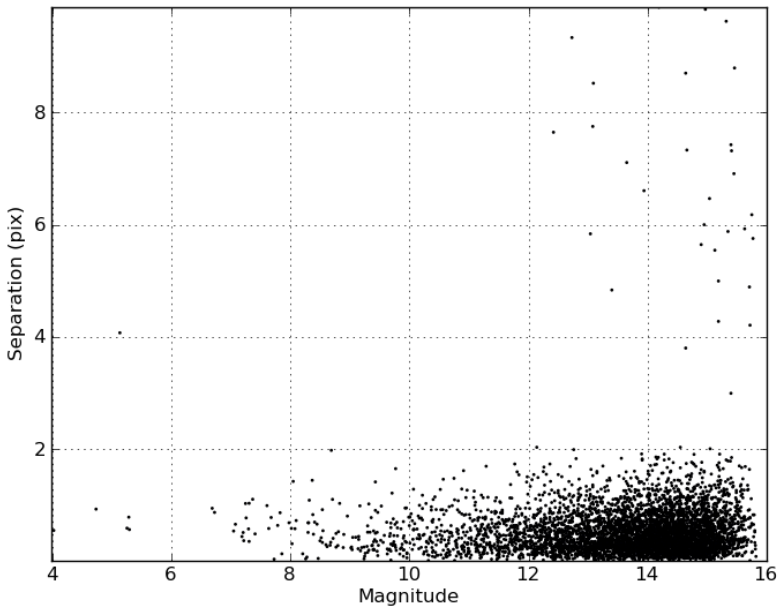

Figure 3.4: Separation between image and catalog positions as a function of magnitude produced using the data for the Astrometry.net calibration of the focused image.

WCS Tools

To successfully use WCS Tools, the inputs must be provided in a particular way. The source file most be ordered in decreasing magnitude and only contain magnitude and position data. The images must also be orientated in a particular way, image north running up the y axis and east running along negative x. Failure to do either of these will at best produce incorrect calibrations and at worse cause the program to crash.

It was therefore necessary to rotate the NGTS prototype images using the "imrot" function in the WCS Tools package to perform successful calibrations. All additional processing steps in the "imwtmc"[9] were also used to give the best possible result. What was quickly noticed was that the tool was faster, taking only three to five seconds, than Astrometry.net. However the plots give a first impression of the tool being less accurate than Astrometry.net though this proved to not be the case, as demonstrated by the Gaussian cross sections. Strangely, the defocused image seems to be more accurately calibrated than the focused.

Figure 3.5 shows the scatter plots for the calibration, the same as with Astrometry.net. Again a y axis bias seems to exist in the focused image though it is not apparent in the defocused image. There might be a slight bias in the x axis of the defocused.

Figure 3.6 and Figure 3.7 indicate that the x axis bias does indeed exist, though it shifts the entire distribution. The astrometric solution of the focused image also has a noticeable bias in the y axis shown by the Gaussian not fitting the histogram as well as in the other plot in Figure 3.6. The full width half maximums for both nights are indicating that WCS Tools can produce a more accurate calibration compared to Astrometry.net, a result that could not be determined had only scatter plots been used, which along with its speed makes it a more appealing candidate.

SCAMP

SCAMP needed an initial WCS approximation and so was tested on images after an initial calibration had been carried out using Astrometry.net.[10] The same analysis was carried out on the astrometric results and plots are produced exactly as before.

[9] This is the 2MASS specific call for the general command "imwcs"

[10] Astrometry.net was chosen over WCS Tools in an attempt to avoid adding large numbers of tool specific keywords to the image headers. One of the optional processing steps used with WCS Tools fitted a quadratic polynomial adding at least 10 additional keywords to the image headers. The distortion calculations by SCAMP would have then added another 10 keywords. This may cause compatibility issues.

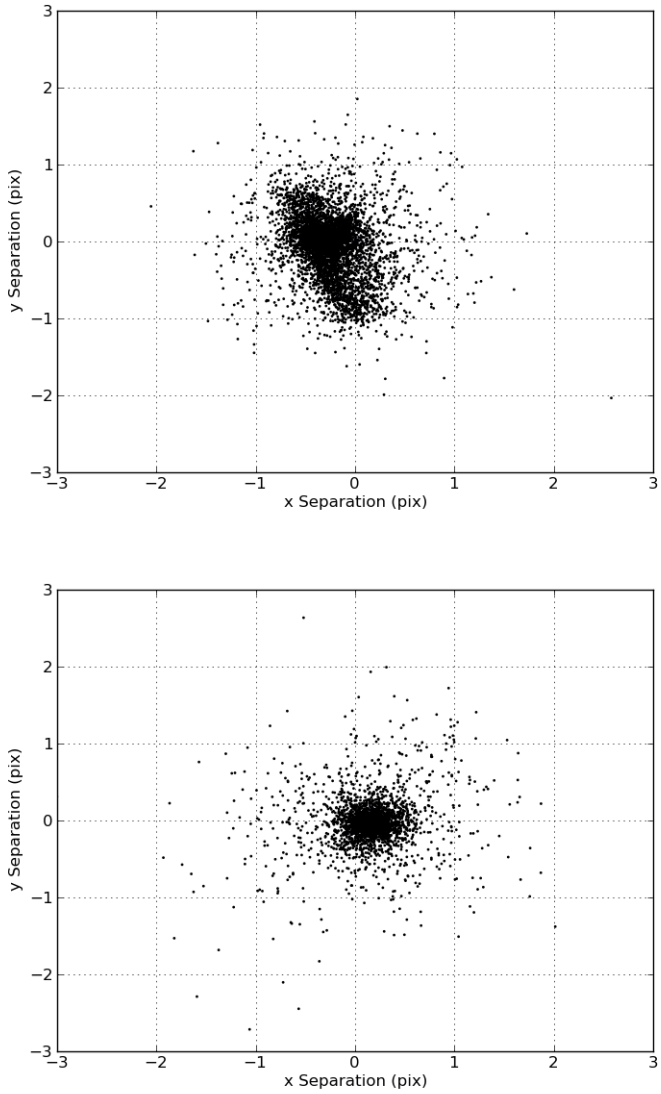

Figure 3.5: Scatter plots for the accuracy of the WCS Tools astrometric solution. Focused (20091007) on the top, defocused (20100204) bottom. The defocused plot displays a tighter main cluster but has more dispersed points. The focused cluster is showing a bias along one direction again.

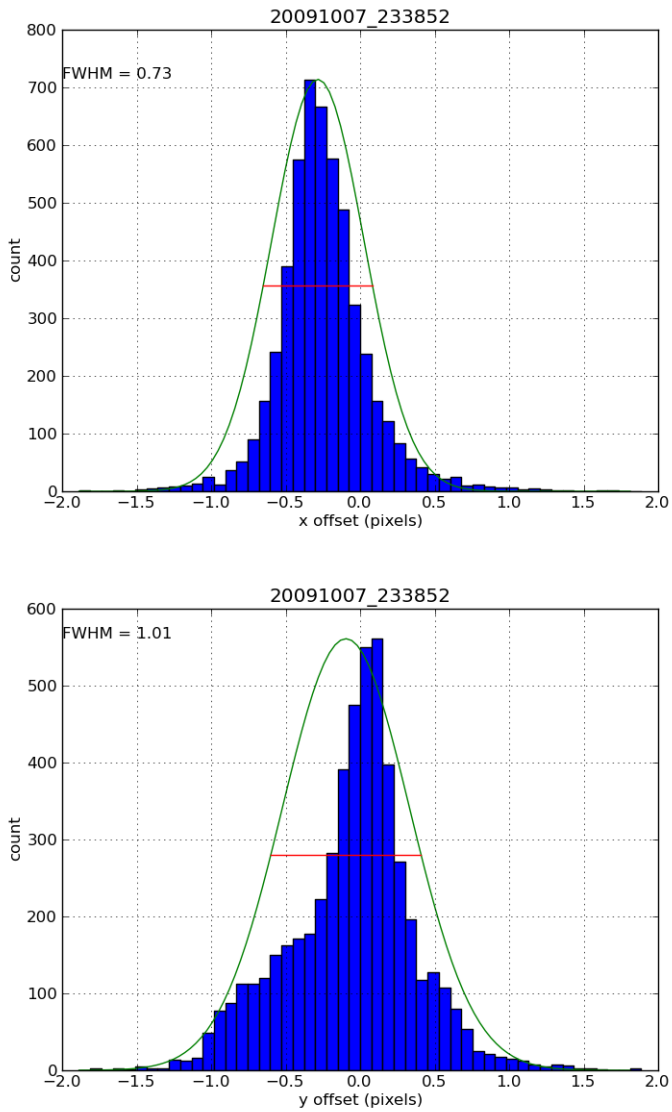

Figure 3.6: Gaussian fits to the cross sections of the top scatter plot (focused) (WCS Tools calibration) in Figure 3.5. The histograms display a more Gaussian distribution.

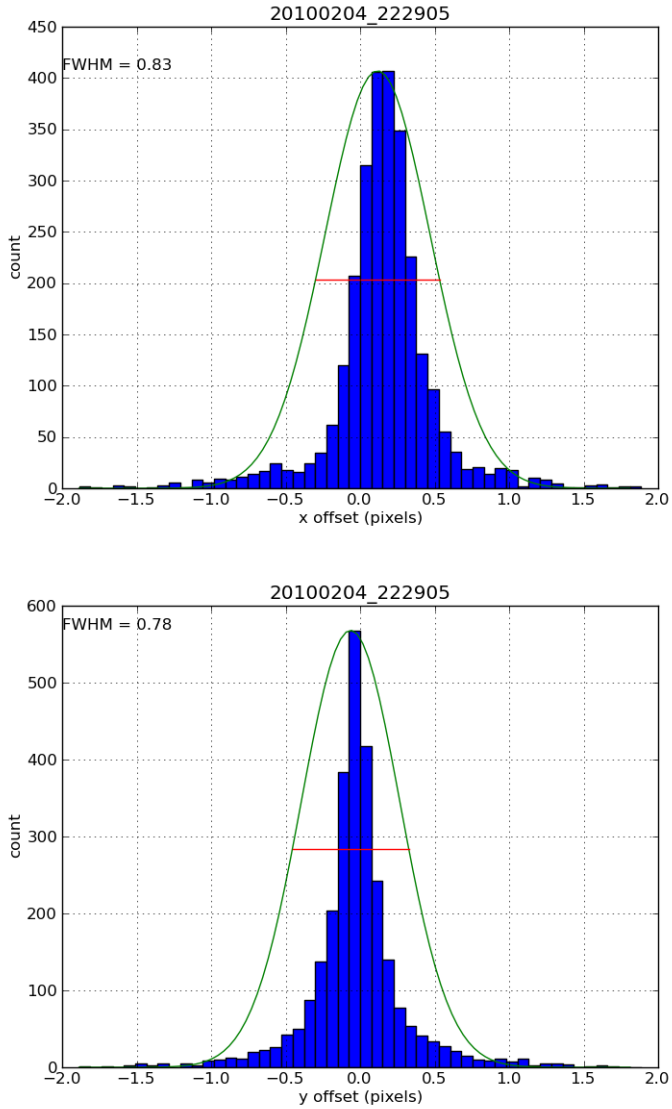

Figure 3.7: Gaussian fits to the cross sections of the bottom scatter plot (defocused) (WCS Tools calibration) in Figure 3.5. There is an interesting improvement in accuracy on the y axis compared to Figure 3.6.

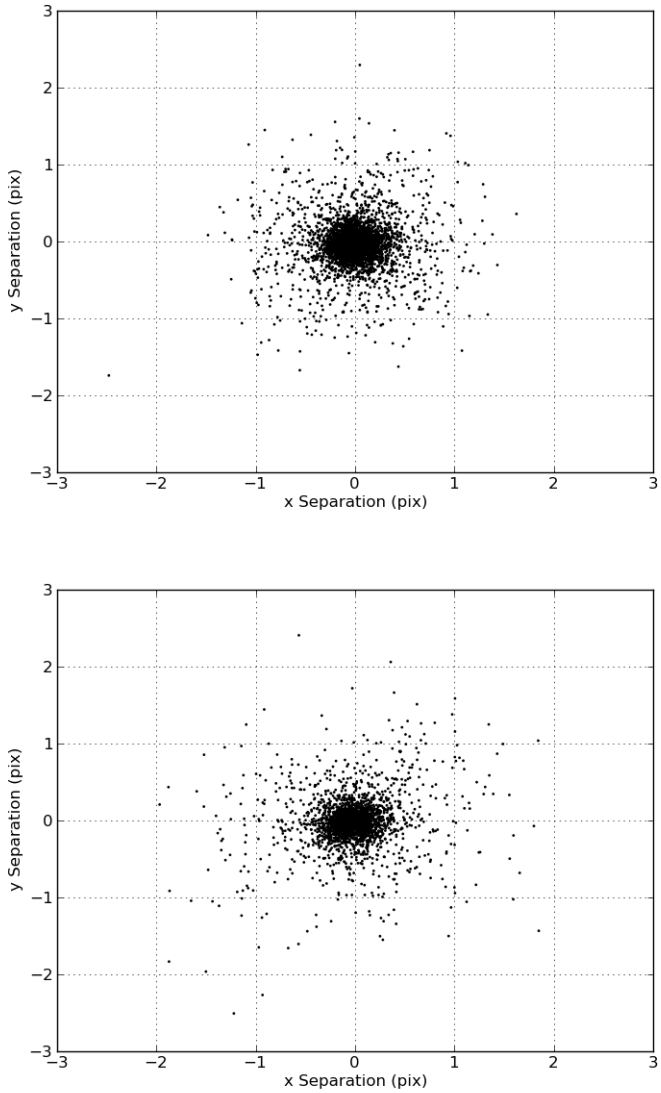

Figure 3.8: Scatter plots for the focused and defocused master images calibrated with SCAMP. Images are those listed in Table 3.1, focused top, defocused bottom. Of interest is the tight clustering and lack of any obvious offset.

Tool	x (pixels)	y (pixels)
Astrometry.net	0.85	1.07
WCS Tools	0.73	1.01
SCAMP	0.61	0.64

Table 3.2: FWHM coordinate uncertainties for the focused image (20091007) for all three astrometric calibration methods.

Figure 3.8 displays the scatter result which indicate the more accurate calibrations possible with this tool. There is no bias and the Gaussian plots will indicate that if one does exist, then it will be very small. The accuracy is better due to the ability to account for the radial distortion in the images.

The scatter and cross section plots in Figures 3.8, 3.9 and 3.10 support this tool as being the most accurate. There is far less outward scatter and more objects are being binned in and around zero. Though not perfect, the Gaussian fits indicate a lack of any major bias along a particular axis.

The main downside to this tool is speed. It can add between three and five seconds to the calibration time already needed by Astrometry.net. This combined with the keywords being obsolete and the need for another astrometric tool and additional libraries makes it a less attractive tool to use despite its accuracy.

Throughout this analysis it has been assumed that a Gaussian profile offers the best fit to the histograms. Clearly this has not been the case as can be seen from many of the fits. The issue is that the histograms tend to be skewed and the plotted Gaussian profiles do not account for this. As the objective was to determine a FWHM for the histograms and in most cases the skew was not readily apparent until after Gaussian fitting, usage of the Gaussian was acceptable. Alternatives that account for skew do exist but, using the log-normal distribution as an example, they only account for skew in one direction meaning different distributions would need to be used on different plots as some are right skewed and some are left skewed.

Table 3.2 lists the FWHMs of the coordinate uncertainties for all the tools for the focused night.

All three tools show a significant error margin in the y axis compared to the x axis. This is less so with SCAMP which produces an overall more clustered result. WCS Tools is slightly better than Astrometry.net overall but as has been repeatedly shown worse than SCAMP. Table 3.3 completes this analysis with the results for the defocused night.

Astrometry.net produced poorer calibration at this focus. The only real additional points of interest here is that WCS Tools and SCAMP achieved better

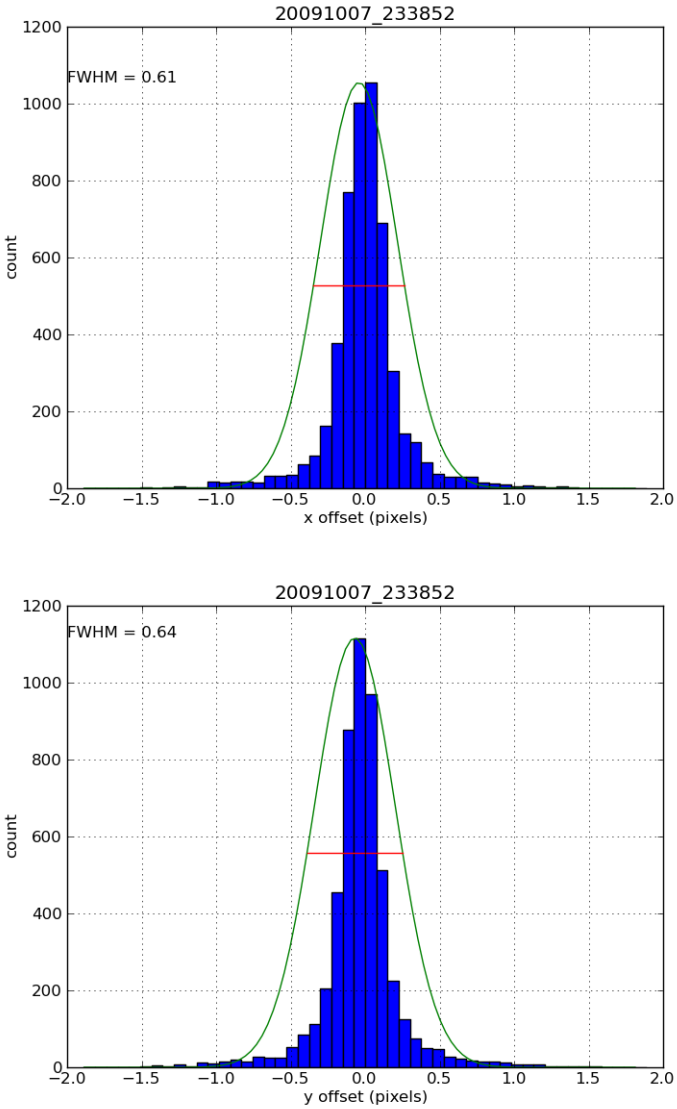

Figure 3.9: Gaussian cross sections for the focused plot (top) in Figure 3.8 (SCAMP calibration). The offset axis is limited in range and there are a few points outside the range as seen from the scatter plots.

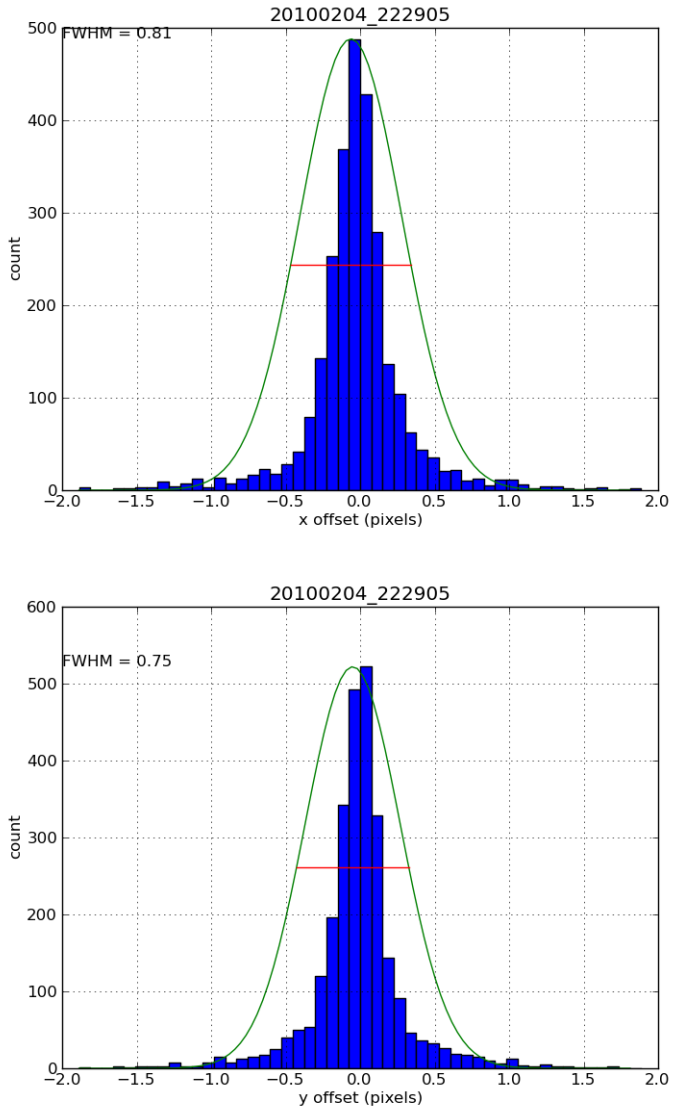

Figure 3.10: Gaussian cross sections for the defocused plot (bottom) in Figure 3.8 (SCAMP calibration).

Tool	x (pixels)	y (pixels)
Astrometry.net	1.04	1.07
WCS Tools	0.83	0.78
SCAMP	0.81	0.75

Table 3.3: FWHM coordinate uncertainties for the defocused image (20100204) for all three astrometric calibration methods.

results in the y axis than they did in the x and WCS Tools achieving a better accuracy under defocused conditions.

3.2.3 Data Set Testing

The testing of the packages was extended to a full meridian of data. The process was automated by incorporating the command line calls to the packages within scripts. The different speeds of the tools was readily apparent here with up to five hundred images being calibrated consecutively. WCS Tools would run through the set within two to three hours whilst both the other tools would take up to ten hours to work. Scatter plots would no longer work as an overall depiction of accuracy. The median offset across all the images would instead be plotted to indicate how the precision of the calibrations changed throughout the data set.

Astrometry.net

Figure 3.11 shows the result achieved with Astrometry.net for the different focuses. There is a significant amount of variation in the precision during the course of the observations for both nights. Slight variations in image quality could be attributed to the small scale variations. The large jump at the end of the focused night corresponds to about the time of the meridian flip. As expected the defocused night is less precise and shows the largest variations.

WCS Tools

If we compare Figure 3.12 which is the results for WCS Tools with Figure 3.11 we see that WCS Tools is more consistent with variations on a much smaller scale. What is interesting is that WCS Tools stays more or less consistent in terms of the calibration whilst occasionally getting a better match on some images, it never really gets worse than its initial offset level. This contrasts markedly with Astrometry.net which can produce calibrations worse than the base line that it achieves. A couple of the early images in each night were calibrated poorly by WCS Tools and this was kept in mind when building the master catalogues for the nights (See Chapter 4).

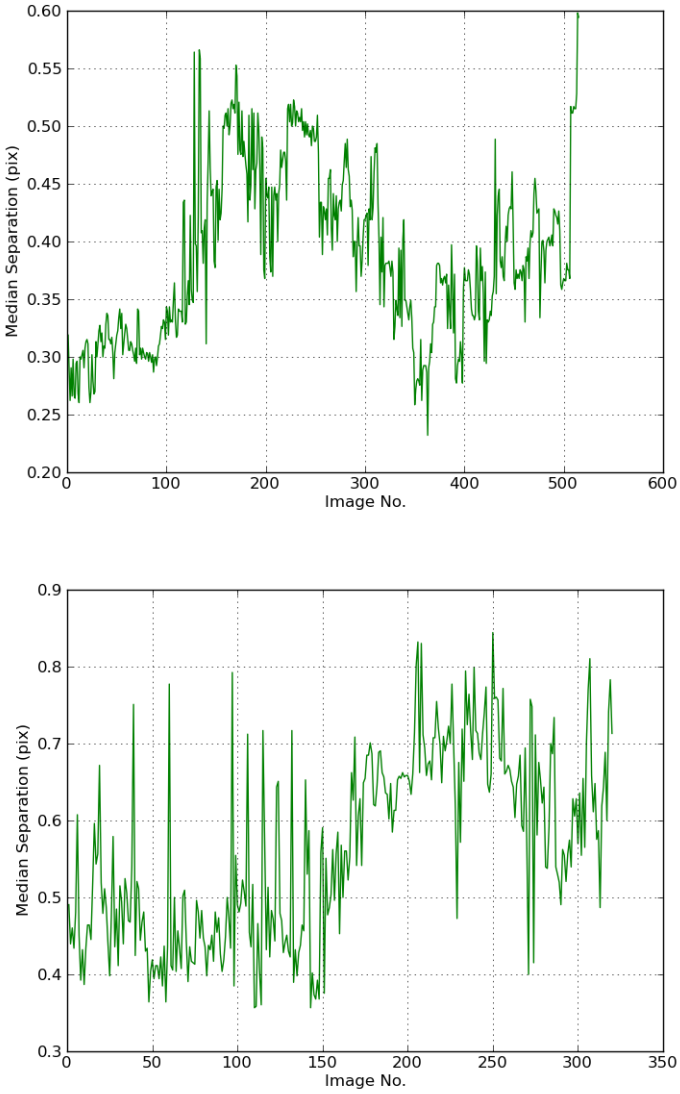

Figure 3.11: All-night precision plots for Astrometry.net. Top plot is the focused night, bottom is the defocused night.

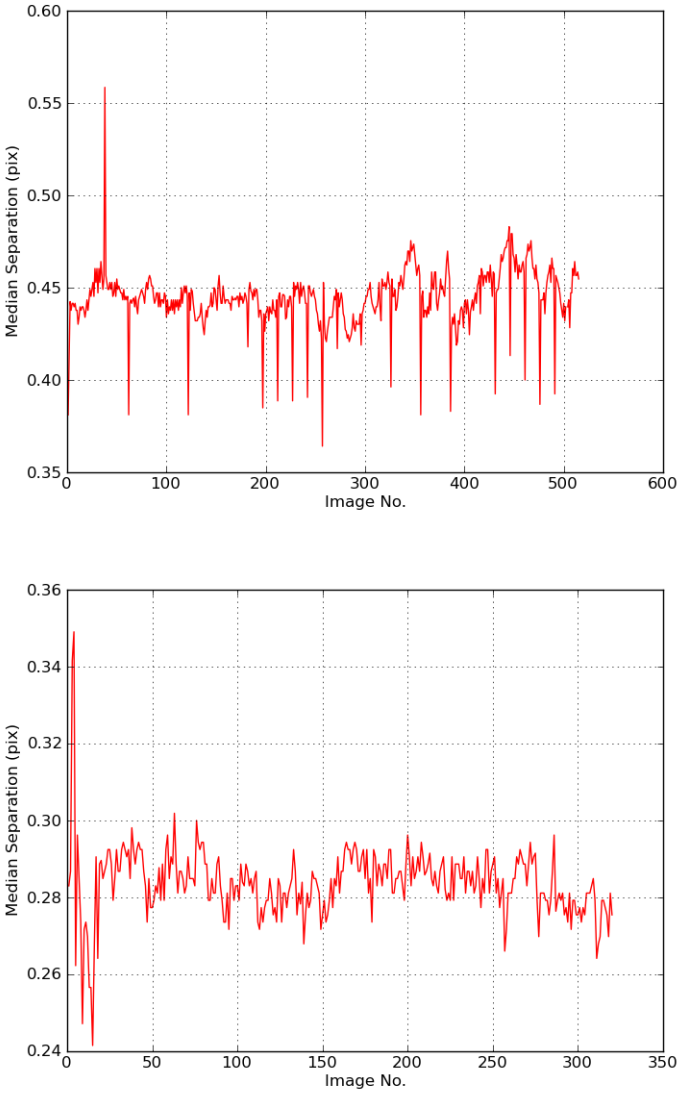

Figure 3.12: All-night precision plots for WCS Tools. Exactly the same nights for focus are used with focused on the top and defocused on the bottom.

SCAMP

Figure 3.13 shows that SCAMP is more accurate with smaller values for the median offsets for each image but is not that precise as the value for the offset varies more frequently though the data set. The precision improves slightly at the cost of accuracy in the defocused calibration, Figure 3.13 bottom plot.

To better compare all the tools with each other the results have been combined into two plots, one for each focus. It shows that SCAMP is definitely the most accurate of the tools but is a bit lacking in precision. Astrometry.net is showing itself to be the worst as it is lacking in both accuracy and precision and, at a poor focus, is by far the worst of the tools. WCS Tools is reasonably consistent and holds the middle ground for accuracy. WCS Tools also shows slightly more precision than SCAMP during its more stable periods. Which of these tools will be used in the final NGTS pipeline will depend on the requirements of the project. However for the rest of this project WCS Tools will be used based on its precision which is needed for easy catalogue creation, speed and ease of use.

3.3 Photometric Calibration

The second stage of the image calibration process was photometric calibration. The zero points of the images have been determined but this only gives an instrumental magnitude. At the same time it was also an aim to build a reference catalogue of all the objects in a field. It was decided to calibrate the images to the Carlsberg Meridian r band though it had to be remembered that the images were not actually observed in this band. This is also not the most suitable band for brighter stars as they see more reddening due to extinction making them appear brighter than they really are in this band.

3.3.1 Catalogue Creation

The calibration process began with the creation of an object catalogue for the field. This was required because each image has its own limiting magnitude. If for example the limiting magnitude for one image was 17.6 and another was 17.4, objects with a magnitude of 17.5 would be detected in the first image but not the second. Therefore a catalogue is needed to list all the objects that could possibly be detected. The catalogue was created using an image stacking tool called SWarp, (from the AstrOmatic software suite) [Bertin et al., 2002]. By stacking a certain number of images the magnitude depth achieved in the catalogue increases, so providing a more

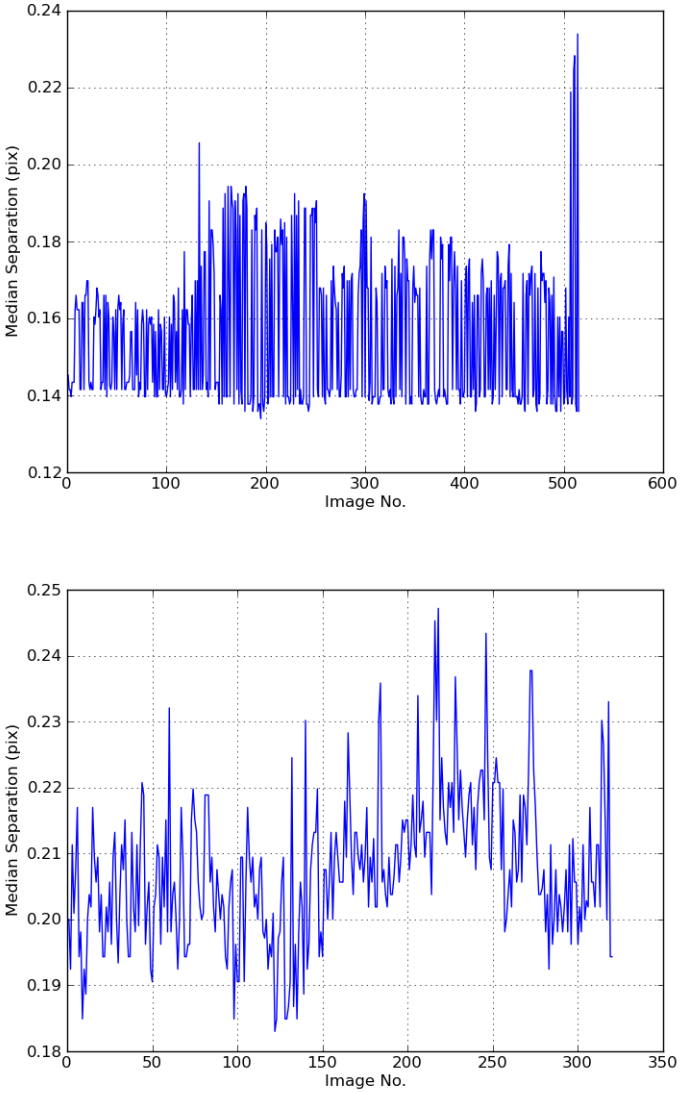

Figure 3.13: All-night precision plots for SCAMP building on an Astrometry.net initial solution. Focused top, defocused bottom.

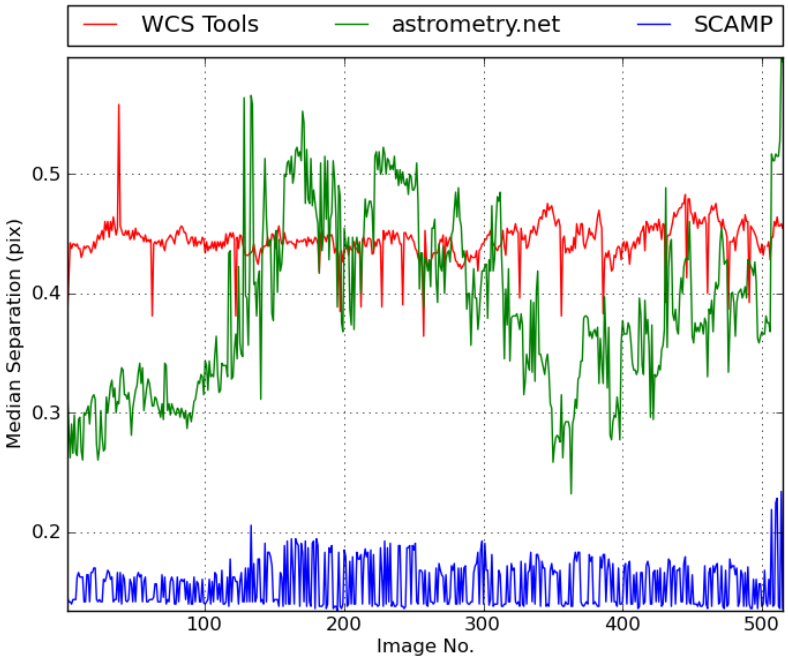

Figure 3.14: Combined precision plots for the night 20091007 the focused night. This clearly demonstrates the accuracy of SCAMP, as the offsets are much lower compared to the other two tools. . The erratic behaviour of Astrometry.net can also be observed.

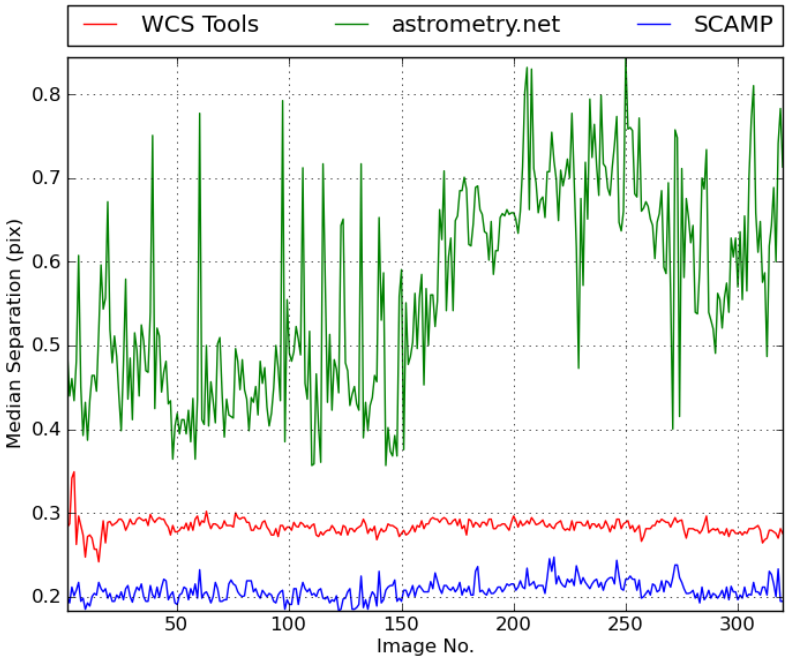

Figure 3.15: Combined precision plots for the night 20100204, the defocused night. (This is the field used for the WASP11 observation see Chapter 4). Astrometry.net and SCAMP both perform worse compared to Figure 3.14. This is a direct comparison of the precision of the three tools.

complete catalogue.

Stacks of ten, twenty five and fifty images were tested to see what could be achieved with co-addition. Figure 3.16 shows histograms of the depth for a single image and for different numbers of stacked images (10, 25, 50). It is clear that diminishing returns are occurring as the number of images used is increased. It is apparent that an improvement of one magnitude is certainly achievable but not a great deal beyond that.

Selecting images can be time consuming as consistent images from the middle of the night are preferred. WCS Tools showed the greatest consistency in calibrations justifying its selection as the calibration tool to used for the rest of my project. The histograms suggest that twenty five images give a significant improvement in depth whilst also not being prone to problems or too time consuming to use. Therefore all master catalogues are created using twenty five consecutive images from the middle part of the night.

Well focused images are preferred for this process given that there will be less smearing of the stars in the image. This is an important consideration as sources extracted from an image produced by stacking multiple defocused images are often treated as multiple blended sources due to the smearing. However, it was possible to build a master with the poor focus night for the WASP 11 transit and work with it so this issue is not as large as it could have been. Figure 3.17 and 3.18 shows the achieved depths for different numbers of stacked images for the defocused night.

The object count is lower for plots in Figure 3.17 and 3.18 compared to Figure 3.16 due to fewer objects being extracted from the stacked images. For the night 20091007 the east meridian is used here and 7500 to 8500 sources are extracted from the stacked masters. On the other hand only 4000 to 5000 objects are extracted from the masters of 20100204.

3.3.2 Pseudo r-band Calibration

To convert the image magnitudes to the Carlsberg Meridian r band the master image was source extracted. The sources were then cross matched against the CMC14 catalogue using a program consisting of a call to Vizier based on the centre of the master image, and STILTS[11] table cross matching routines. STILTS is a Java package with a variety of table manipulation and cross matching functions. For the successful matches the difference between the image and catalogue magnitudes is determined and then the median of this is calculated. The median offset value is then used to adjust all the image magnitudes in the master catalogue. Figure 3.19 shows

[11] http://www.star.bris.ac.uk/ mbt/stilts/

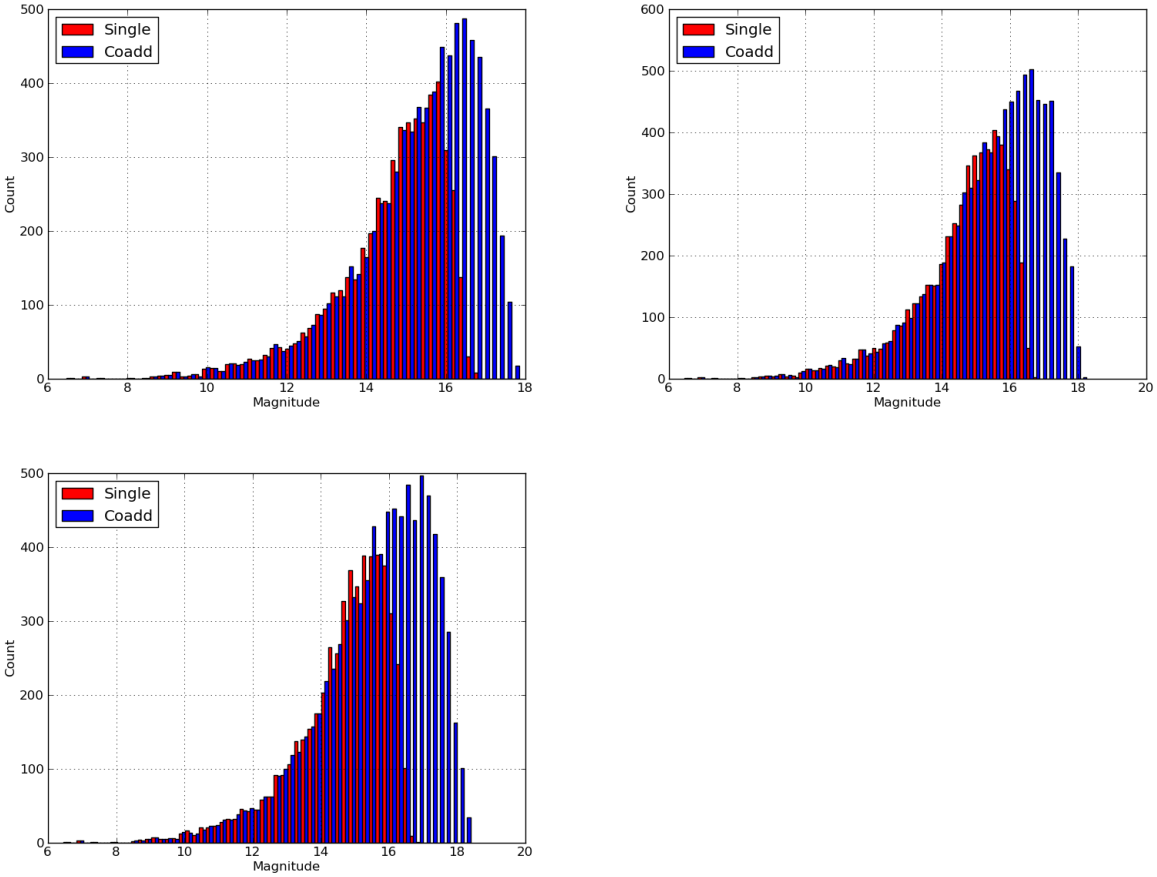

Figure 3.16: Histograms of the number of objects detected as a function of instrumental magnitude for a single image (red) and sets of 'stacked' images. The plots are for a stack of ten (top left), twenty five (top right) and fifty (bottom left) images respectively.

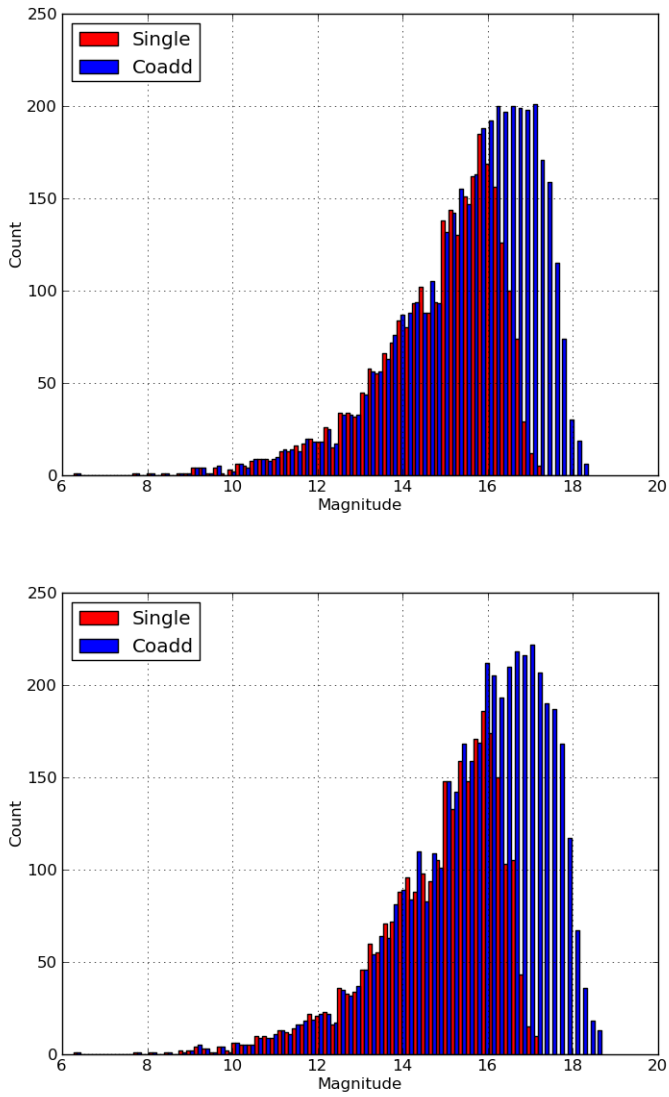

Figure 3.17: Histograms of the number of objects detected as a function of instrumental magnitude for a single defocused image (red) and 'stacked' images (blue). 10 (top) and 25 (bottom) stacks are shown in this figure with stacks for 50 and all images available for the defocused night in Figure 3.18.

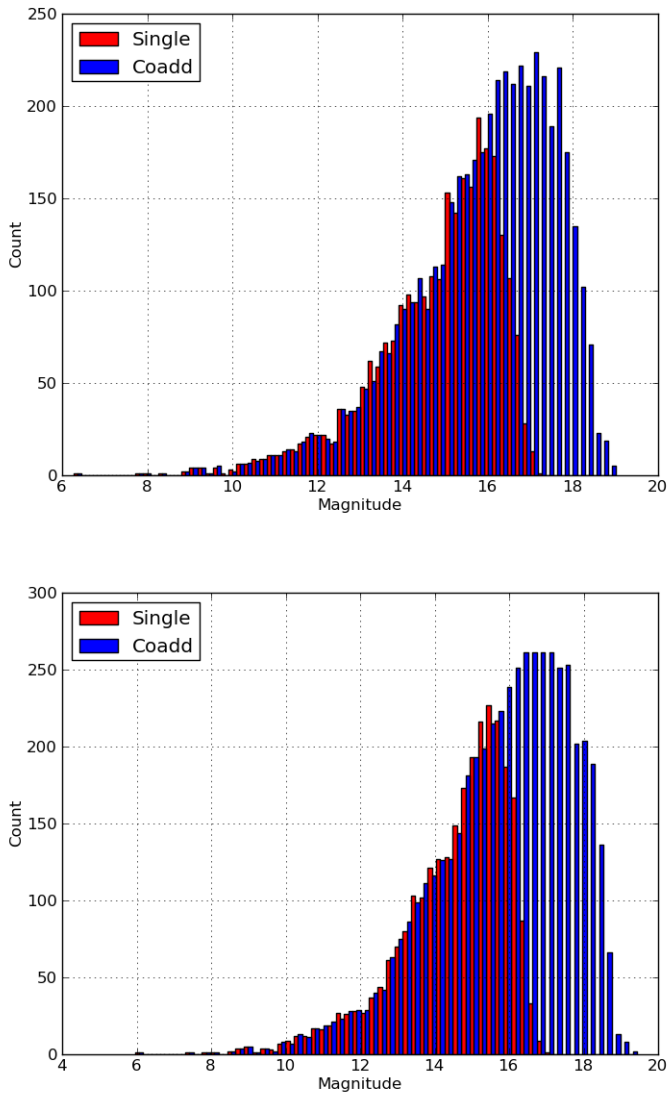

Figure 3.18: Histograms of the number of objects detected as a function of instrumental magnitude for a single defocused image (red) and sets of 'stacked' images (blue) using stacks of 50 (top) and all available images (bottom) from the defocused night.

a comparison between magnitudes in one such master and its relevant Carlsberg Meridian data set. The fit is pretty consistent up to about 16th magnitude and then begins to disperse a bit more. There are a few outliers that could be mismatched objects from master image creation.

Initially the offset calculated for the master was also applied to each of the images. This would work under photometric conditions but the images were not necessarily observed under such conditions. This was made readily apparent during the search for the WASP-11 transit. Figure 3.20 illustrates the issue. The downward spike in the top plot in Figure 3.20 is due to image specific variation in the observing conditions which photometric calibration is intended to filter out. This was rectified by determining a calibration for each image in the night by taking the acquired Carlsberg master and cross matching every object in each image with it and then deriving an offset for each image. This produces a list of offsets for each image in a data set that is then easily applied to all the source data files providing a correction to the calibration. The second plot in Figure 3.20 is again WASP-11 after this calibration had been carried out. This plot still shows some variability as it is the WASP-11 transit which will be studied later (see Chapt.4 Sec.4.4).

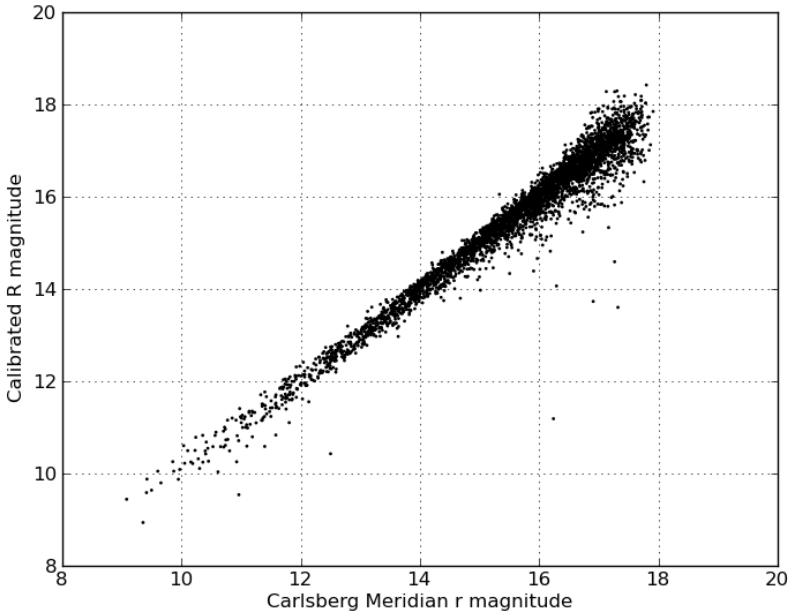

Figure 3.19: Comparing the calibrated r band for each object with its Carlsberg Meridian catalogue r band. The night used in this plot is the east meridian of 20091119, which is one of the nights in field 1 and of significant interest to this project. There are just over 4000 objects matched in this plot.

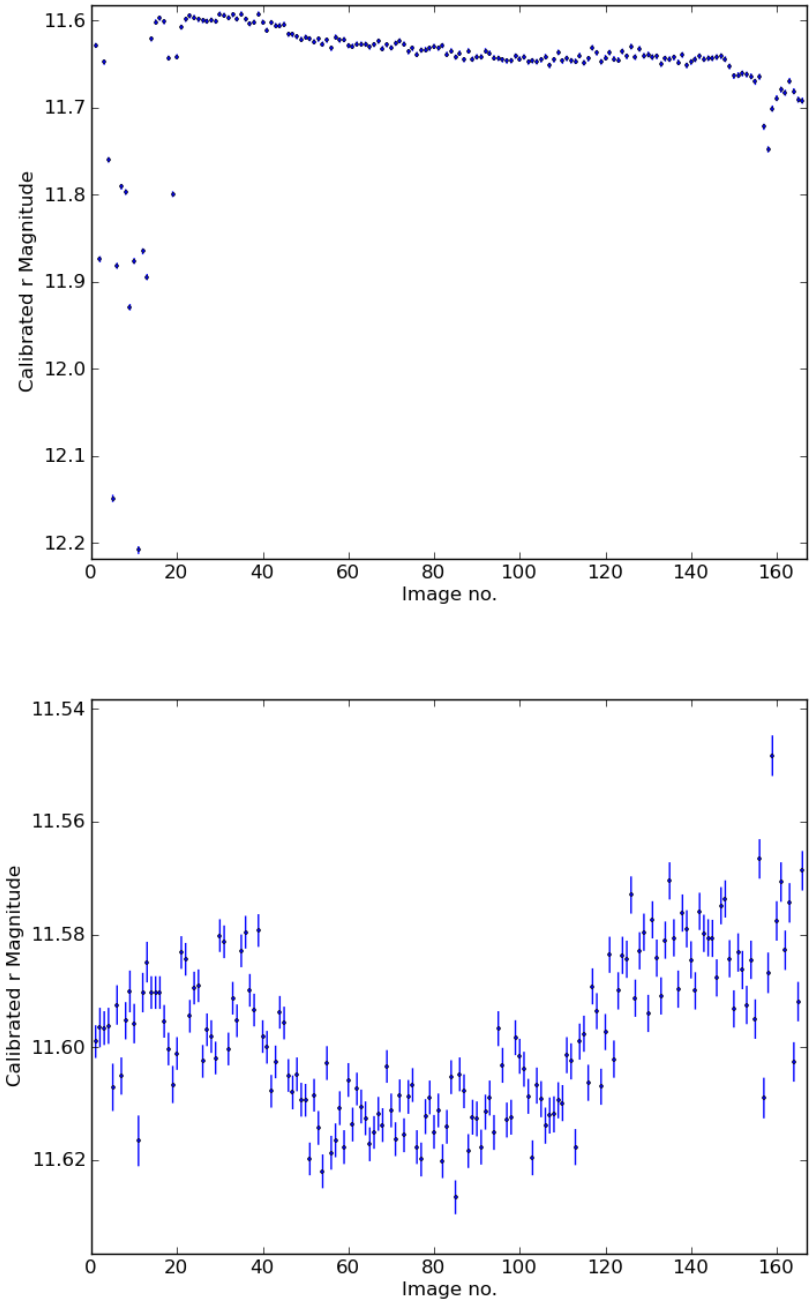

Figure 3.20: Plots showing the results of global calibration for an entire night (top) which would work under photometric conditions (which did not occur) and calibrating every frame (bottom). This is demonstrated using the WASP-11 transit which is why even the image by image calibrated light curve still exhibits variability (see Chapt.4 Sec.4.4)

Chapter 4

Variability

The scientific interest of this project is to characterise the stellar population of the NGTS prototype data. This is split into two areas, variability, covered in this chapter, and classification by stellar type, covered in Chapter 5. Having calibrated the images, as outlined in Chapter 3, it was possible to create light curves for the various sources detected in the images.

4.1 Light Curve Generation

As part of the calibration process master catalogues had been created for each field and observation night. These contained a complete list of all identifiable objects in a field down to about 18th magnitude. Each image of a data set was source extracted, with the sources then cross matched against the relevant master catalogue for that data set. This identified each object in the images, allowing the data across all images to be collated for each object, producing a light curve.[1]

Matching with the master catalogue allowed each object to also gain J, H and K magnitudes from 2MASS, which will be used in the next chapter. There is a significant difference between the number of sources extracted from a master image and from a single image. Taking the good focus test image from Table 3.1, and the associated night, Table 2.2, as an example, approximately 8000 sources were extracted from the master with only 4000 being extracted from the single image. It is clear from this that many of the faintest stars that were discovered by image stacking are unlikely to be recovered from individual images. It is also clear that

[1]The source extraction was carried out using SExtractor and was applied to each image in isolation. The numerical identifier for sources in one image would not be consistent with sources in another image. Therefore each image required cross matching against the master and the fixed numerical identifier for sources in the master is used to identify each source within an image.

sources on the detection threshold of single images are going to lose data points due to the slight fluctuations in the maximum depth achieved from image to image.

The combination of short exposure times and long observation periods imply that each light curve would be expected to have between 300 and 500 data points. It was therefore decided that any light curve with less than 20 data points would be filtered out.

4.2 Identifying Variable Objects

For each data set between 3000 and 5000 light curves were produced. All nights within Table 2.1 were studied. Visual inspection of the light curves could identify any object with significant variability but a more analytical approach would be required to identify smaller scale variability. To determine whether an object is variable its light curve was subjected to a reduced χ^2 test. The formulation is presented in Equation 4.1. This reduced χ^2 test tests a data set against a model and in this specific case the model is that the star has a constant brightness in r defined as $< r >$.

$$\chi^2 = \sum_{i=1}^{k} \left(\frac{< r > - r_i}{\sigma_i} \right)^2 \times 1/N \tag{4.1}$$

r_i and σ_i are the individual magnitudes and errors respectively and N is the number of data points. Under Equation 4.1 an object that has a reduced χ^2 of 1 is not variable and a variable would be identified as an outlier on a plot of reduced χ^2 against magnitude.

The values were calculated and a plot of χ^2 against magnitude was created for the test night, Figure 4.1. Two significant features are of interest. Firstly there is the increase in χ^2 at lower magnitude values. For bright objects the statistical errors on the magnitude are small so any systematic trends, such as airmass, produce a high χ^2.

It was possible to carry out an airmass correction using the VARTOOLS[2] [Hartman et al., 2008] implementation of SYSREM [Tamuz et al., 2005]. SYSREM is a tool for correcting systematic effects in photometry, for example those related to airmass and extinction. For a set of observations the residuals for each observation would be the average-subtracted stellar magnitude, the stellar magnitude after subtracting the average stellar magnitude for the data set. An extinction coefficient for each star is determined via a linear fit to the residuals as a function of the corresponding airmass to the observation. The product of the extinction coefficient and

[2] www.astro.princeton.edu/ jhartman/vartools.html

Coordinate	r Magnitude	χ^2
J005756.233+475655.71	14.0394	3.0037
J005307.090+474029.91	15.0221	1.9957
J005814.306+501644.46	15.6155	2.2129

Table 4.1: Data for a small selection of variable candidates from the night of 20091007.

airmass can then be removed form the residuals thus removing the effects from the data. This can be extended to other systematics effects using the same principles as the extinction coefficient and airmass do not need to be related to the true extinction or airmass, they just need to variables that causes the greatest linear variation in the global sum of the residuals. Usage of this tool required inputting all light curves for a data set as simple files containing only modified Julian date, magnitude and magnitude error. An additional airmass file for the data set was also needed. Finally command line parameters giving values for saturation magnitude and sigma clipping are needed.[3] Figure 4.2 shows the impact of the airmass correction on the χ^2 plot.

The second feature is the individual points well above the main trend with large χ^2 values. These are the variable candidates. Figure 4.3 shows the two light curves of two candidates along with two stars from the main body of the χ^2 distribution in Figure 4.4.

The analysis outlined above only corresponds to one meridian of observations and so it would be possible to extend the curves into the second half of the night adding the opportunity of determining the period of the variability for some objects. Unfortunately for this particular night the reacquisition of the field after the meridian flip was not accurate. The second meridian is off by at least a frame, 1.8 degrees of declination, so no stars match across the meridian. To carry out a proper period analysis a consistent set of observations on the same field over multiple nights would be ideal.

However, stars for both meridians of the night display variable behaviour and data for a small sample are displayed in Table 4.1 and the curves are plotted in Figure 4.5 and Figure 4.6.

[3]The output file for each light curve consists of the original data and a model light curve of that data created from the impact of airmass. Subtracting the model curve from the original data produced the correction. Magnitude values were then restored using the value for that object contained in its master catalogue.

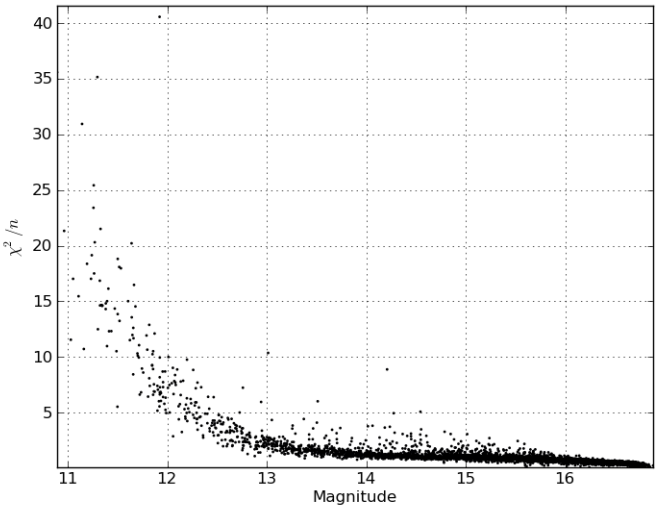

Figure 4.1: χ^2 plot for 20091007 East meridian. The y axis is reduced χ^2. No airmass correction has been carried out and the steep rise visible at brighter magnitudes is related to systematic uncertainties. The outlier in the top left exhibited variability in its light curve. (See Fig. 4.3.)

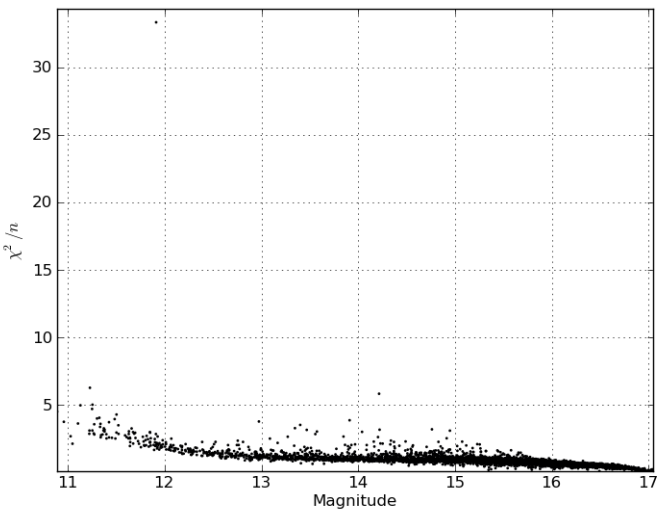

Figure 4.2: χ^2 plot for 20091007 East meridian after application of an airmass correction. The steep rise at the bright end is reduced, but not eliminated completely suggesting that other systematics might still exist. The outlier identified in Figure 4.1 is still clearly visible.

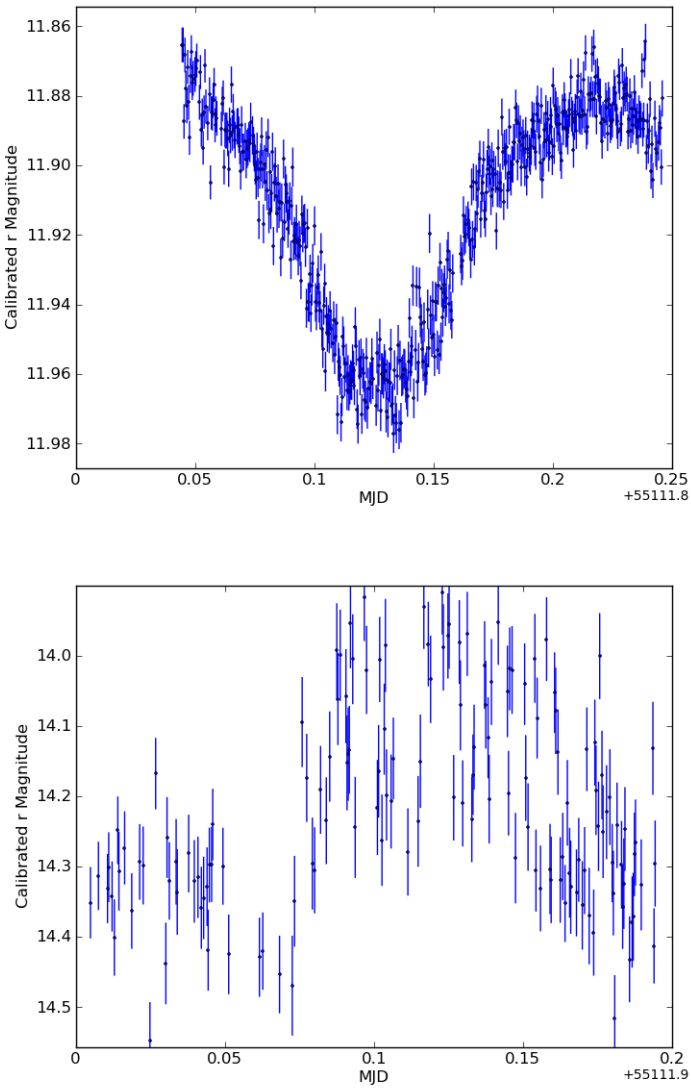

Figure 4.3: Two variables with χ^2 values of 33.3 (top) and 5.8 (bottom). Coordinates are J005303.41+470647.81 (top) and J005745.619+481733.53 (bottom). The top curve is the object with the largest χ^2 value in Figure 4.2.

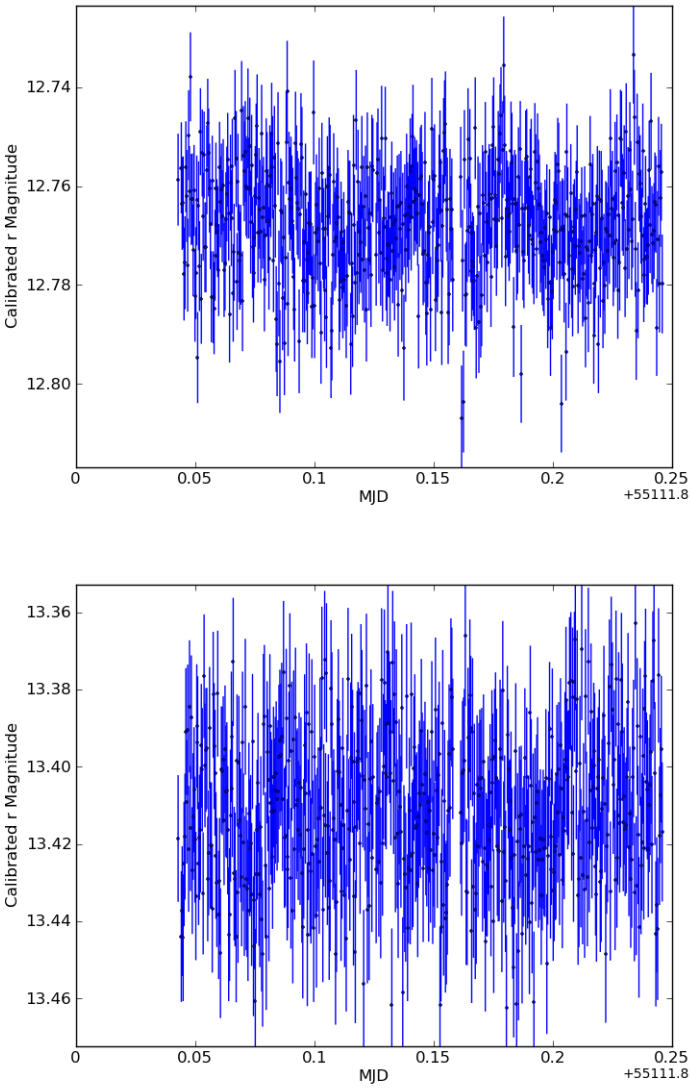

Figure 4.4: Two objects with constant brightness from the same night as Figure 4.3. χ^2 values are 1.3 (top) and 1.1 (bottom). Coordinates are J005820.037+472403.75 (top) and J005219.507+480457.43 (bottom).

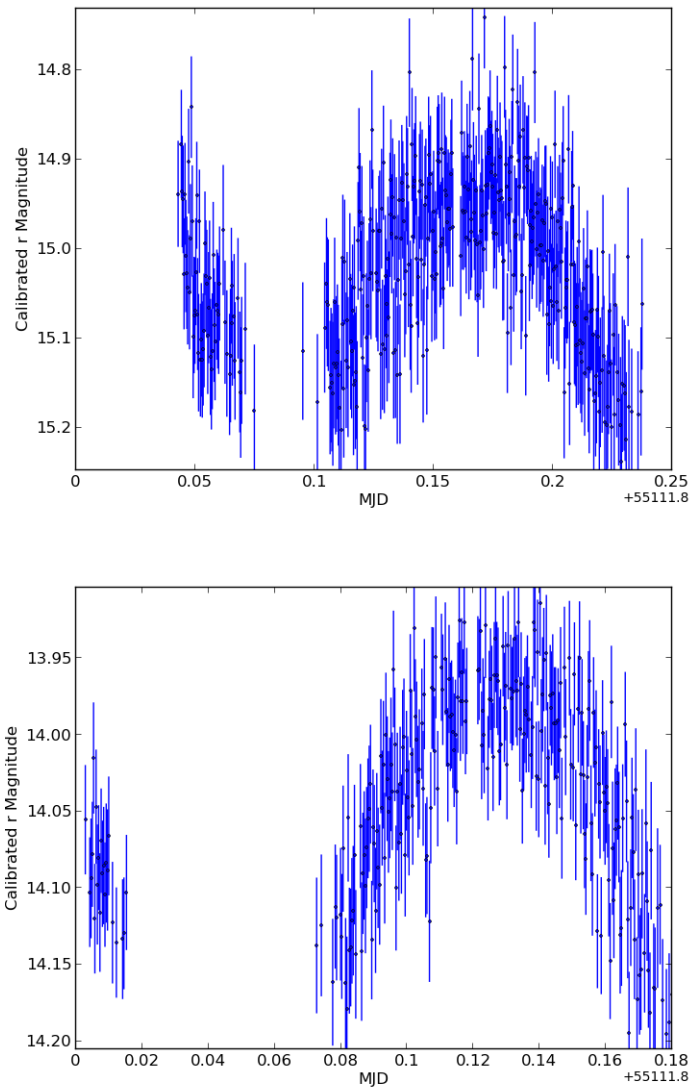

Figure 4.5: Two objects from the first half of the night 20091007 taken from Table 4.1. Top curve has coordinates J005307.090+474029.91 and bottom has coordinates J005756.233+475655.71.

4.3 Time Series Analysis

Table 2.2 identifies several nights of data that were taken focused on the same field and are identified in the table as Field 1. Three nights of observations at 30, 60, 120 and 300 second exposure times were taken, but as discussed in Chapter 2 only the nights in Table 2.2 were of sufficient quality.

The nights at 120 and 300 second exposure times all suffered from significant saturation. The two later nights at 60 seconds were discarded due to the moon affecting observations and a different, nearby field being observed instead. The nights in Table 2.2 consist of eight meridians and all were calibrated astrometrically and photometrically as described in Chapter 3. The night of 20091121 had suffered severe weather problems, leading to the closing of the dome on two occasions, and this impacted the quality of the light curves, leading to the night being discarded. One meridian of data from each of 20091129 and 20091209 was also found to be of reduced quality and discarded. In total four good meridians were available for time series analysis.

SYSREM airmass corrections were applied to the light curves using airmass values for the relevant meridians. From this, variables were searched for using the χ^2 method described above. Objects that showed a large value for χ^2 for their magnitude, determined by comparison with objects of similar magnitude, were then inspected visually to check the implied variability.

To determine the period of the variable objects multiple nights would be needed as the observations of the objects needed to be longer than their periods. It was therefore necessary to link the light curves from each meridian with each other. Each master catalogue contained 2MASS position data for the objects and this was used for cross matching as it would be an identical property in each master catalogue.

The cross matching demonstrated the fact that not every object had been detected in each night. In Table 4.2 the number of objects within each master for each meridian used is given. The second half of the table shows the number of objects existing across multiple nights and this value decreased as more nights were used.

Figure 4.7 shows a good quality variable from field 1 which will be used for discussing the methodology of the period analysis. Due to the gaps between the individual nights the curve is shown in several sections. The behaviour of the light curve would suggest an eclipsing binary or ellipsoidal modulation. The star was observed over a sufficiently long period to enable a detailed period analysis.

Night	No. of Objects
20091119 East	4996
20091119 West	4166
20091129 East	5030
20091209 West	2414
Nights	No. of objects matched
20091119 East, 20091119 West, 20091129 East, 20091209 West	394
20091119 East, 20091119 West 20091129 East	1465
20091119 East, 20091119 West	1896

Table 4.2: Table containing the numbers of objects listed in the master catalogues for the nights used in Field 1. The bottom 3 entries are the number of objects identified to have data in all the listed nights.

A time series analysis software suite implemented in MIDAS was employed to search for periodicity in the data. It allows testing of the curves under a variety of techniques. Four different methods were available for the period analysis.

4.3.1 The Software

The methods can be divided into two sets. One set is better suited to sinusoidal variations and the other works best for non-sinusoidal modulation. The first method is called "power" within the software. This method performs a discrete Fourier transform to determine period. The second method, "scargle", that is best applied to sinusoidal data computes a Scargle periodogram. For a full description see [Scargle, 1982].

The two methods that perform better with non-sinusoidal modulations are analysis of variance, (aov), and a method described as "ort". Analysis of variance takes a test period and phase folds the light curve over this period. The phases are binned and a χ^2 test is applied. The closer the test period is to the real period of the curve the more phases are binned correctly and the result of the χ^2 test increases. A full description is available in [Schwarzenberg-Czerny, 1989].

The final method, "ort", is based on the aov method, but fits sine curves to the phase folded data and tests the accuracy of said fits. Again a full description of this method can be found in [Schwarzenberg-Czerny, 1996]. All of these methods are called via the command line within the software. All the methods require a frequency range to test over and a defined number of test frequencies. For the analysis of my light curves the range was chosen from zero to twenty cycles per day (d^{-1}) as most of the variability to be tested is observed to be on a short time-scale with multiple cycles per day, with 10000 test frequencies. The "ort" method also

needs the number of harmonics used in the sine fits to be defined, in my case this was set to two.

All the methods would produce a periodogram, such as the one in Figure 4.10 from which the highest peak could be selected as the period. The light curve data is then phase folded over this period producing a plot such as shown in Figure 4.11. The two colours in the phase plot correspond to the separate nights of the curve in Figure 4.7, and if the determined period is accurate enough, the two colours will exactly overlay.

4.3.2 Application

All four methods were applied to the light curve shown in Figure 4.7 and periodograms and phase folded light curves for each method are presented. The first method applied is "power" and the periodogram is presented in Figure 4.8. By selecting observations close together an attempt had been made to reduce or eliminate the issue of aliases. These aliases arise due to uncertainty in the number of cycles that have passed between the nights. This shows up in the periodogram as the lack of a single clearly defined peak. The separation between the various peaks would be one over the gap in observations in days. Using Figure 4.8 the highest point is determined at 7.5136d^{-1} but there are several aliases as shown by the zoomed in plot in Figure 4.8. This peak gives a value for the period of 0.1331 days.

Figure 4.9 is the result of phase folding the data shown in Figure 4.7 over a period of 0.1331 days. The black points correspond to both meridians of 20091119 and the red points are from 20091129. The overlay of the red onto the black is poor, especially when compared with results from the other methods shown below.

The second method applied was "scargle". Figure 4.10 shows the periodogram which is almost identical to Figure 4.8, which is not surprising, as both methods perform very similarly on a curve displaying a quasi-sinusoidal variation. The highest peak is found at 7.5156d^{-1} which again gives a period of 0.1331 days.

Figure 4.11 is the result of phase folding the "scargle" result. This figure is obviously also very similar to Figure 4.9, and again is not the best possible result when compared with the better results from the remaining two methods.

Analysis of variance was next to be applied to the light curve. The periodogram in Figure 4.12 has two significant peaks offering two possibilities for the period. The first peak is at 7.7148d^{-1} giving a period of 0.1296 days, similar to that found from the previous methods. The result of phase folding over this period is shown in Figure 4.13 left plot and is of similar quality to that achieved using the other two methods.

The other peak in Figure 4.12 is at 3.708d^{-1} giving a period of 0.2697 days. This is roughly twice the length determined by the other methods so far. Figure 4.13 right plot is the result of phase folding over this period,and provides a much better alignment of the data for the two individual nights than that achieved using the "power" and "scargle" methods suggesting that 0.2697 days is more likely the period of the object.

Finally the "ort" method was applied producing the periodogram in Figure 4.14. In this case the highest peak is at the shorter frequency of 3.808d^{-1} though a second also exists. Following from what was discovered with the "aov" method only this peak is considered. This peak gives a period of 0.2626 days and the result of phase folding is in Figure 4.15.

Figure 4.15 has a good overlay of the second half of the data, in red, over the first, in black. The period determined, 0.2626 days, with two peaks and two troughs within one phase cycle is physically plausible. In the case of an eclipsing binary within one cycle there would be two instances when one star is obscured and two instances when both are visible, resulting in two troughs and two peaks respectively. If the observations of an eclipsing binary cover an entire phase cycle it is possible to make assumptions on the characteristics of the system. If the troughs have different depths than it can be assumed that the surface brightness of the two stars are different. When the fainter of the two stars is obscured the trough is shallower compared to when the brighter is obscured. As with exoplanets the period of the system sets a value on the separation of the two stars, shorter period indicating a close or even contact binary pair whilst a longer period would imply a greater separation between the stars.

Ellipsoidal modulation involves a rotating star with elliptical shape. A simplified visualisation is presented in Figure 4.16. The observed variation in magnitude is attributed to the changing visible surface area presented to the direction from which the star is viewed. Peaks in its cycle correspond to viewing with the semi-major axis, hence larger surfacer area, presented towards the observer and troughs correspond to the semi-minor axis, thus smaller surface area, being viewed by the observer.

4.4 WASP11 Transit

The main purpose of the NGTS project is the search for planetary transits. Therefore some of the prototype testing was devoted to observing the transit of WASP11. On 4th February 2010 images were acquired of a field that included WASP11, full

details on that night are available in Table 2.2.

The data from this night has already been used repeatedly within this project. The night was observed with the instrument defocused and the data was used in Chapter 3 for testing the various astrometric calibration tools on defocused images. Additionally the object identified as WASP11 is used in Figure 3.20 to demonstrate the differences between a global photometric calibration and an image by image calibration.

As was briefly covered in the photometric calibration section this observation of the WASP11 transit is a key example of the difference between performing a global calibration or an image by image calibration. As was shown in Figure 3.20, had only a global calibration been carried out, the WASP11 transit would have been obscured in the original data. Clearly this night had not been observed in perfect photometric conditions. Any detrending work that would then have been carried out was likely to display features that would reduce the quality of the light curve. By undertaking the image by image calibration a light curve with much better quality is produced, as shown in the top plot of Figure 4.17, which can then be de-trended to improve the overall quality.

The transit light curve is shown in Figure 4.17 along with an improved plot acquired by applying SYSREM to the data. The transit depth is about 2%. Figure 4.18 displays the WASP11 observation from [Brát, 2009], the top plot is of more interest to our analysis. Comparing Figure 4.18 with Figure 4.17 shows agreement on the transit depth which is about 2% in the comparison figure as well. Both have clearly defined beginning and ending to the transit with the same transit time, 0.1 axis unit.

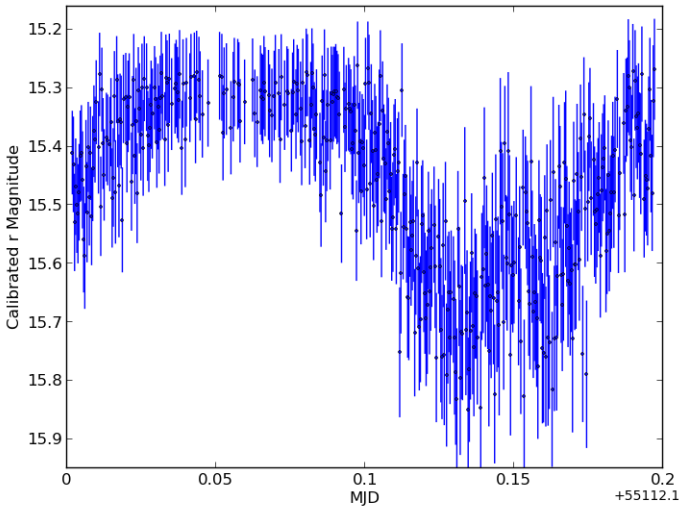

Figure 4.6: Third object from Table 4.1 with coordinates J005814.306+501644.46 taken from the second half of the night 20091007.

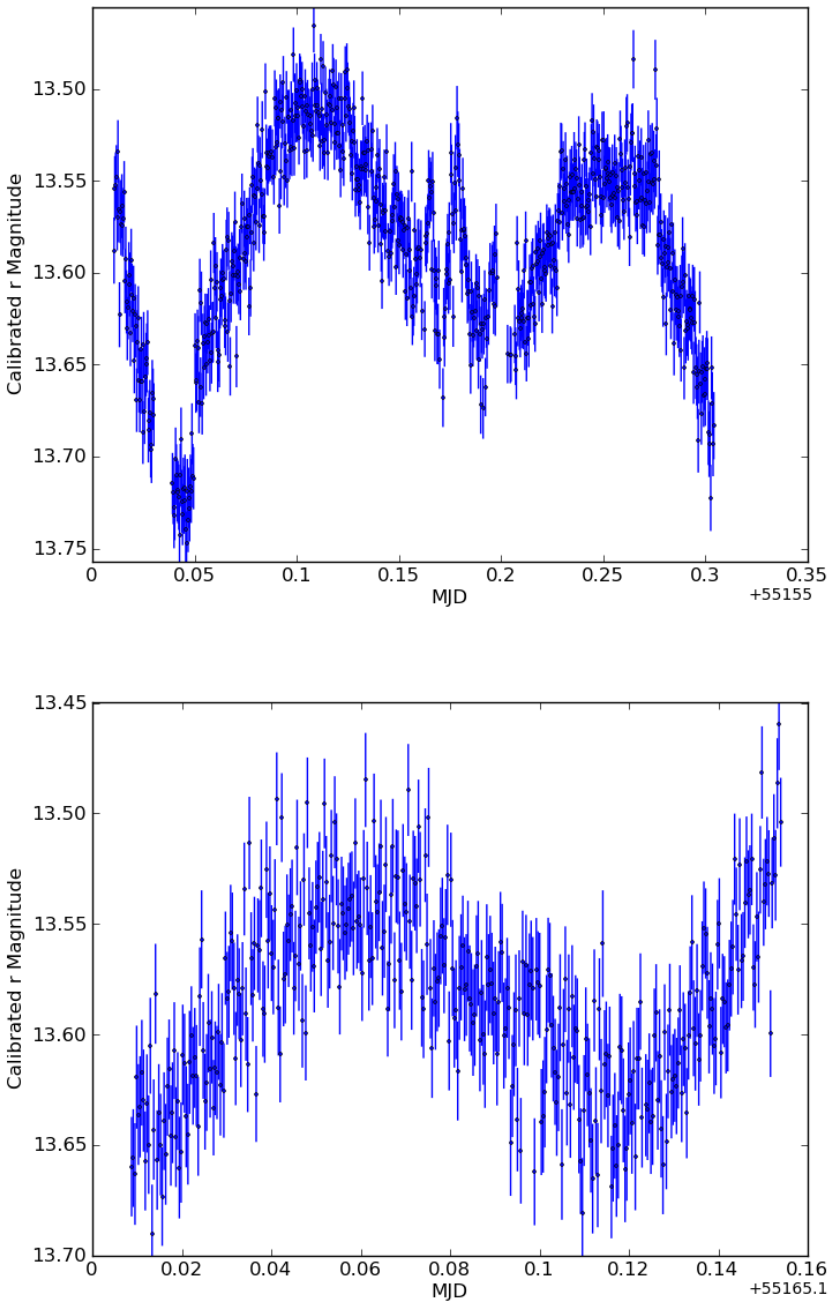

Figure 4.7: Variable from field 1. Curve is presented in two parts due to the ten day gap between the observations. The curve has a χ^2 of 13.36, and coordinates: J062529.576+411620.91.

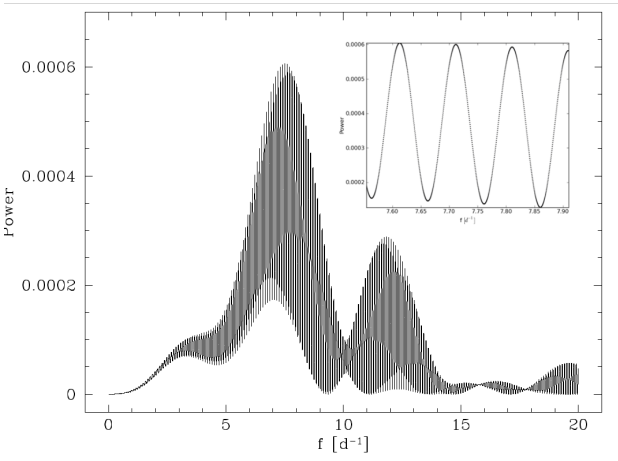

Figure 4.8: Periodogram for the Fourier transform determination of the period for the light curve in Figure 4.7. Included is a plot zoomed in on the leftmost peak highlighting the aliases which occur.

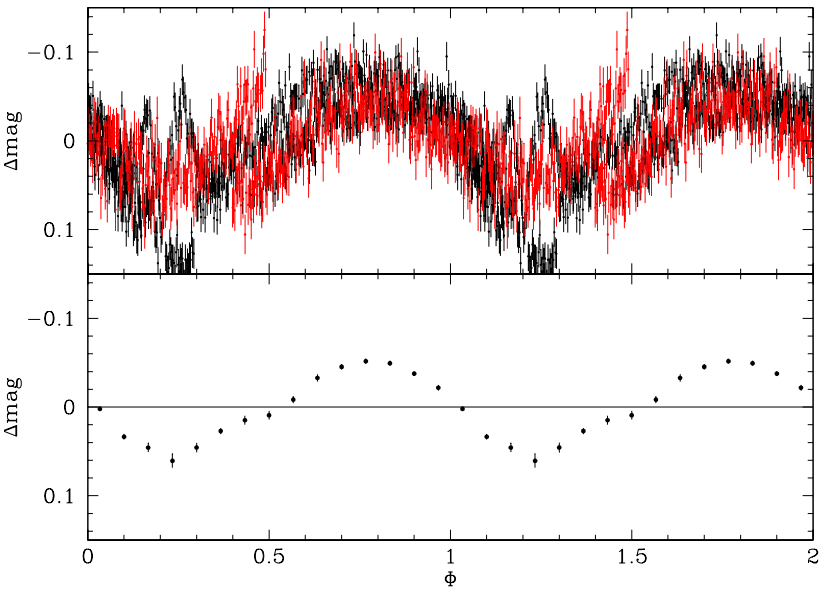

Figure 4.9: Phase folded light curve over the period, 0.1331 days, as determined from Figure 4.8. The period was determined using the "power" (Fourier transform) method.

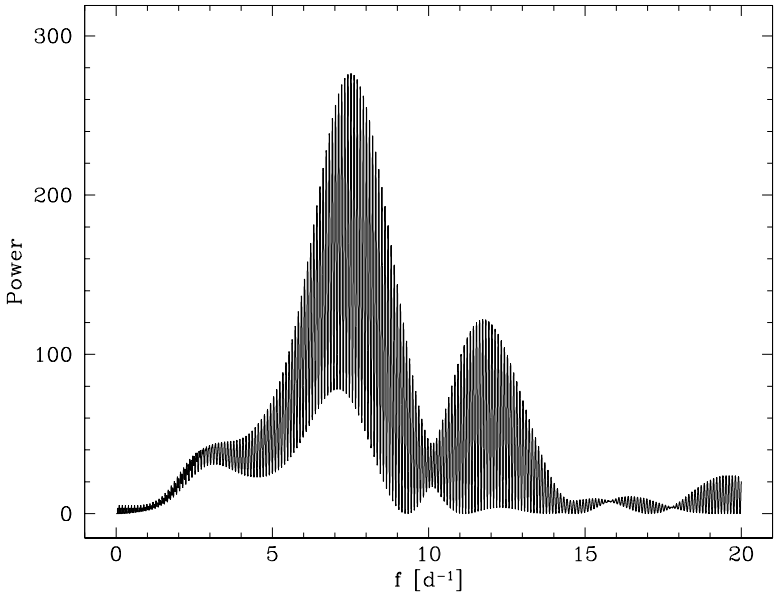

Figure 4.10: Scargle periodogram for the light curve in Figure 4.7.

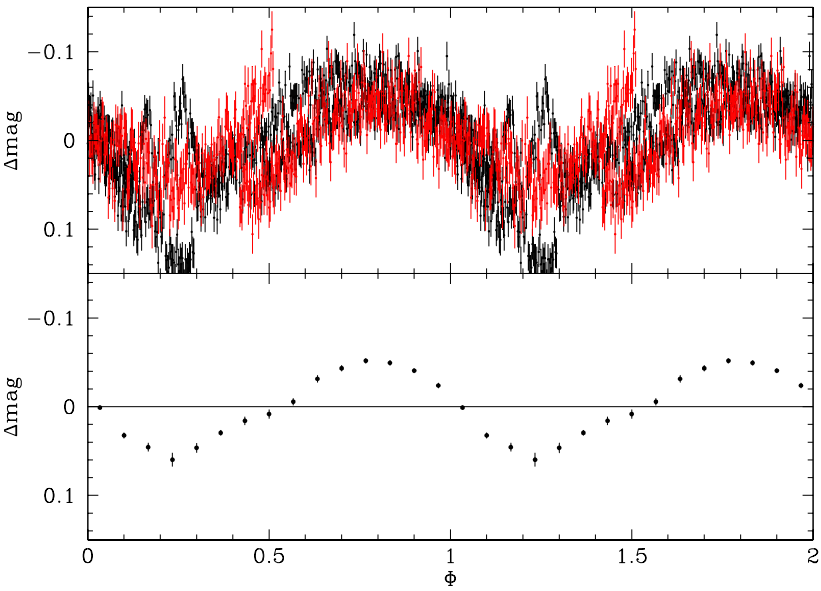

Figure 4.11: Phase folded light curve using a period of 0.1331 days, as determined from Figure 4.10 which used the "scargle" method.

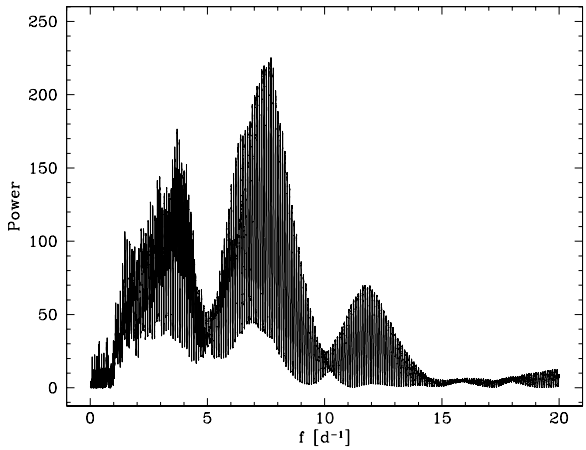

Figure 4.12: Periodogram for the aov method. Two significant peaks are visible, one at 3.708d^{-1} and the other at 7.7148d^{-1}, and both were phase folded. This is for the light curve in Figure 4.7.

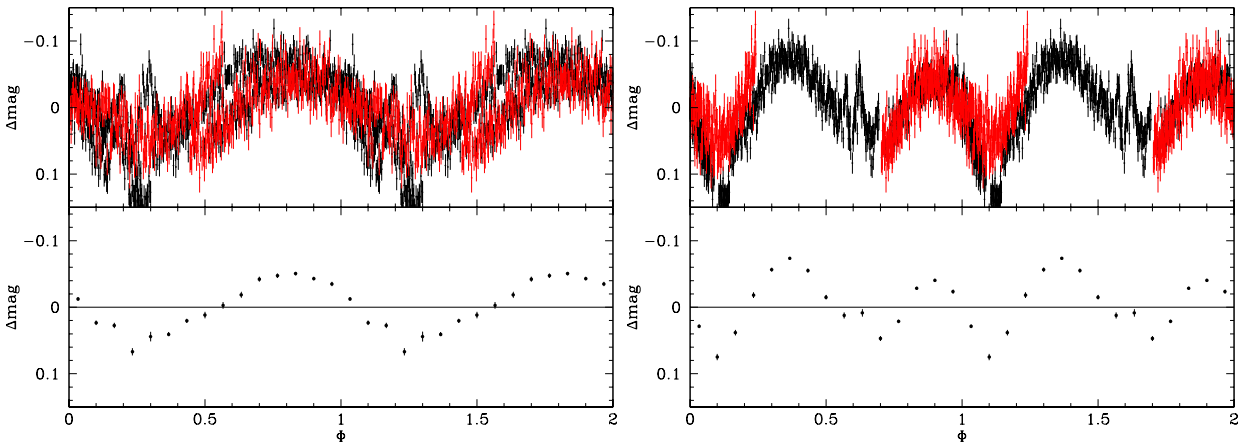

Figure 4.13: Phase folded light curve over a period 0.1296 days determined from Figure 4.12 which was derived from the peak at 7.7148d^{-1}(left). Phase folded light curve using a period of 0.2697 days which was derived from the peak at 3.708d^{-1} identified in Figure 4.12(right).

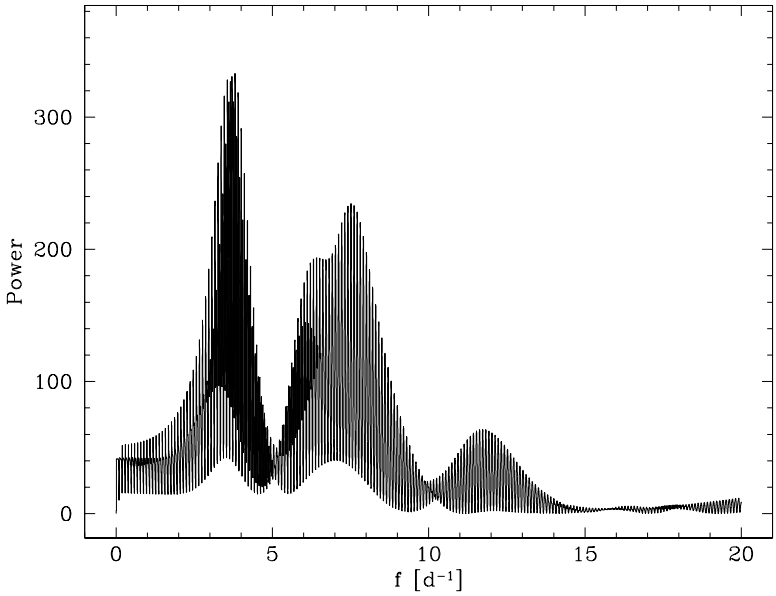

Figure 4.14: Peridogram for the ort method applied to the light curve in Figure 4.7.

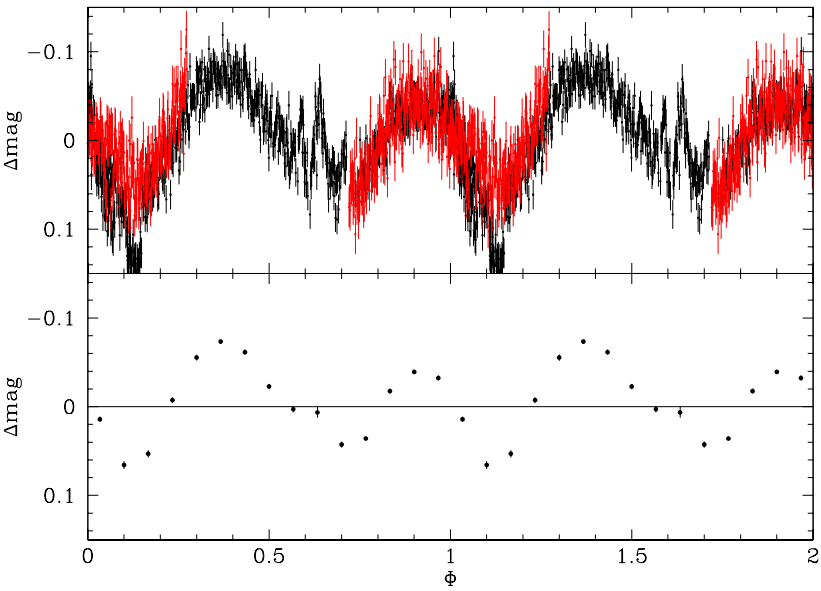

Figure 4.15: Phase folded light curve using a period of 0.2626 days derived from the peak at 3.808d^{-1} in Figure 4.14.

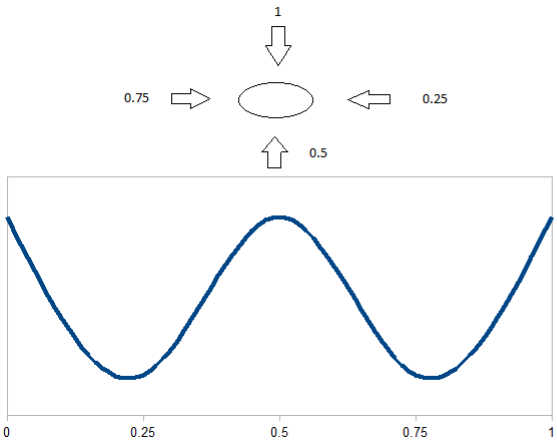

Figure 4.16: Simplified visualisation of ellipsoidal modulation. The arrows correspond to our direction of view at various points during the phase cycle.

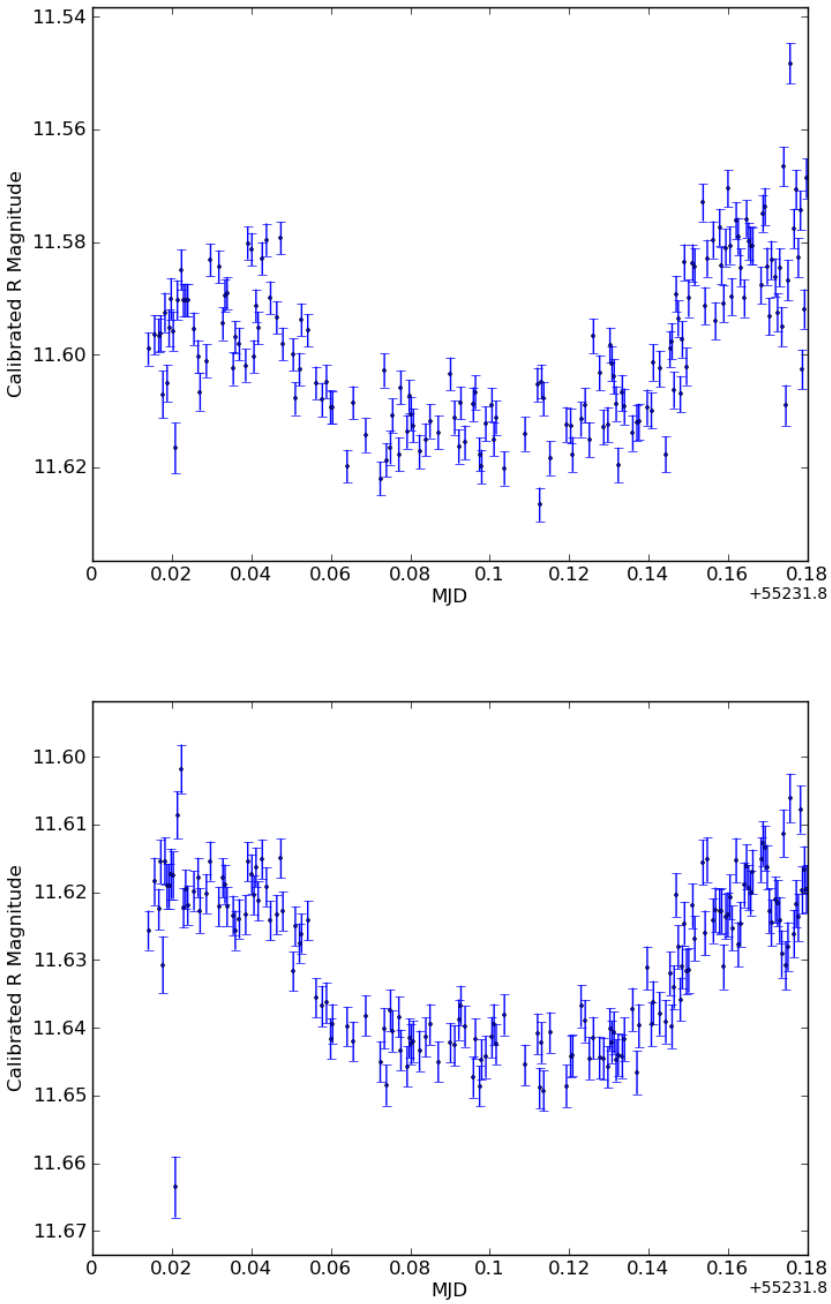

Figure 4.17: The WASP11 transit both before (top) and after (bottom) SYSREM corrections were carried out.

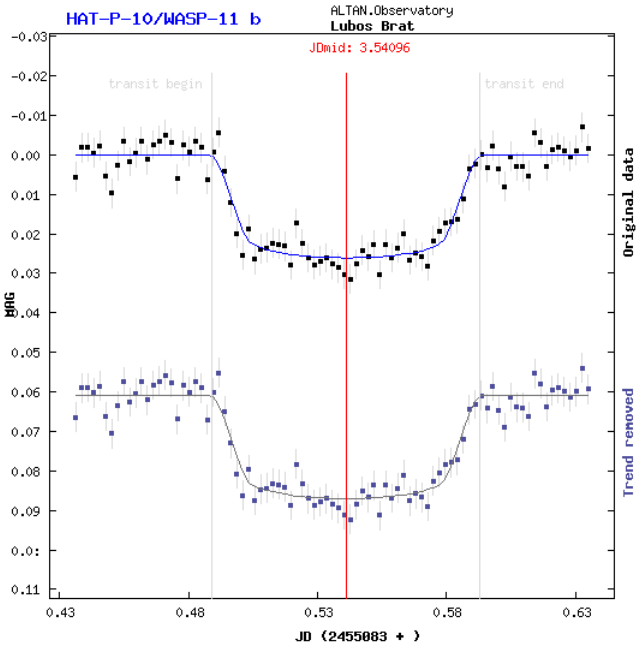

Figure 4.18: Light curve of an observation of the WASP11 transit from 2009 [Brát, 2009]. Used for comparison with my own WASP11 plot.

Chapter 5

Characterisation

The study of variability is only part of the process of characterising the stellar population observed. Determining the stellar types and linking them to the variability information is equally important, especially in regards to M dwarfs. M dwarfs are of particular interest as they have become a major focus for planetary searches, as their study promises the detection of smaller planets, that would produce undetectable transits around the G-type stars that have so far been the focus of exo-planet searches.

5.1 M Dwarfs

With this interest in M dwarfs, identifying them within the NGTS prototype data was a priority. The methodology adopted follows the large study of M dwarfs by Lépine and Gaidos [2011]. The method applies colour cuts and a reduced proper motion cut to separate M dwarfs from other spectral types and to remove giant contamination from the selection. The colour cuts were made using 2MASS J, H and K band magnitudes and the same can be applied to the NGTS prototype data as cross matching between the NGTS fields and 2MASS has been carried out in Chapters 3 and 4.

The colour cuts applied are listed in Equations 5.1, 5.2, 5.3, 5.4 and 5.5.

$$J - H < 0.85 - 0.6(H - K_S) \tag{5.1}$$

$$J - H > 0.72 - 1.2(H - K_S) \tag{5.2}$$

$$J - H > 0.40 \tag{5.3}$$

$$H - K_S > 0.10 \tag{5.4}$$

$$H - K_S < 0.40 \tag{5.5}$$

Applying these to field 1 objects, see Table 2.2, selects objects in the region identified in Figure 5.1. The objects selected are, just as was found by Lépine and Gaidos, likely to include some giant contamination. These needed to be filtered out.

In the work by Lépine and Gaidos the filtering of giants was achieved for stars with parallax information by performing an absolute magnitude cut. The NGTS prototype data lacks parallax information so this method could not be used. Instead the method used by Lépine and Gaidos for stars which lacked parallax data was applied. This involved calculating the reduced proper motion of the stars using Equation 5.6. In this equation μ is in arcseconds per year. Reduced proper motion can be used as an analogous property to the absolute magnitude in the absence of an accurate distance determination. The proper motion act as a proxy for the distance, as objects near to us have a larger parallax and a larger proper motion and more distant objects have smaller values for parallax and proper motion. This allows a mathematical connection between the two quantities which is presented in Equation 5.7 where υ_T is the transverse velocity.

$$H_V = V + 5log\mu + 5 \tag{5.6}$$

$$H_V \equiv M_V + 5log\upsilon_T - 3.38 \tag{5.7}$$

Figure 5.2 shows the stars from the survey covered in Lépine and Gaidos (2011) plotted using their reduced proper motion. From this a cut could be applied based on reduced proper motion and colour and is shown in Equation 5.8.

$$H_V > 2.2(V - J) + 2.0 \tag{5.8}$$

Unfortunately this cut is in V whereas the NGTS data is calibrated to a 'pseudo' r band, (Chapt.3 Sec.3.3.2). Using the data for the stars with parallax data from the Lépine and Gaidos paper, provided on request by the authors, an attempt was made to determine a cut replacing V band magnitudes with r. The stars with parallax data were used due to the clearly defined separation between dwarfs and giants visible in Figure 5.2. To acquire r band magnitudes for these objects, they were cross-matched against the Carlsberg Meridian catalogue. Only a small number of matches was achieved due to the stars being bright, J $<$ 9, M dwarfs.

The reduced proper motion plot, using r, for these stars is shown in Fig-

ure 5.3. A clear separation between dwarfs and giants is not readily visible from this plot. The failure to have two clearly defined populations can be attributed to viewing the population in the red end of the spectrum. When L*é* and Gaidos studied their data they discovered a modest population of very red M giants in their operating magnitude range. By operating in the red end of the spectrum these bright giant sources appear to be closer and have a reduced proper motion similar to the fainter and actually nearer M dwarfs thus removing any separation between the populations. Determining a cut to filter out giant contamination did not progress beyond this point and the probability that M dwarf candidate lists contain some giant contamination was accepted.

One additional colour cut based on r was still sought though. Attention turned to several other papers, West et al. [2011], and Pickles [1998], all of which contained spectral data, especially for M dwarfs. Study of these allowed the identification of a simple cut based on r and J presented in Equation 5.9. This cut is also apparent from Figure 5.3 as indicated by the blue line which includes all the M dwarfs.

$$r - J > 2 \tag{5.9}$$

Applying this cut to an initial M dwarf candidate selection, obtained using cuts in J, H and K, for the focused test night, Table 3.1, produced a reduced M-dwarf candidate list. Figure 5.4 is the reduced proper motion plot of this list. Comparing this with Figure 5.2 would suggest that three candidates with the smallest values of H_r are in fact giants, and giant contamination is expected.

Only limited study into variable M dwarfs has occurred and, whilst variability of M dwarfs makes planet searches difficult, M-dwarf activity is an important issue for the habitability of planets around M dwarfs. Therefore a search for variable M-dwarfs was undertaken. Using data from the nights in field 1, Table 2.2, all the colour cuts in Equations 5.1, 5.2, 5.3, 5.4, 5.5, and 5.9 were applied. Figure 5.5 is the reduced proper motion plot for the final candidate list. One object might be a giant. Cross referencing the candidate list with data acquired in Chapter 4 on variability did not uncover any significant variables.

The magnitude distribution for the M candidates was investigated and is presented in Figure 5.6. Three of the objects are clearly brighter than the rest and so warranted a brief investigation using SIMBAD[1]. The brighter two of the three were found to be K stars, the brightest a K2 and the other a K0. The third object was not

[1] simbad.u-strasbg.fr/simbad/

Spectral Class	R-J Cut
O	-0.57 to -0.54
B	-0.54 to -0.17
A	-0.17 to 0.35
F	0.35 to 0.7
G	0.7 to 0.93
K	0.93 to 2.00

Table 5.1: R-J cuts for spectral classes as applied to field 1 objects

Spectral Class	Number	Percentage
O	0	0
B	3	0.06
A	46	0.92
F	100	2.00
G	300	6.00
K	4330	86.67
M	127	2.54

Table 5.2: Class distribution for field 1 objects for a total of 4996 objects.

given a classification within SIMBAD. This demonstrates that a K contamination exists within the M dwarf candidate list along with giant contamination.

5.2 Other Stellar Types

The papers from which the R-J cut for M dwarf identification was derived from also contain data for other spectral types. This made it possible to determine additional R-J cuts for other spectral classes and gain a rough idea of the distribution of spectral types in the observed fields. This was applied to field 1 using the cuts listed in Table 5.1. The numbers for each class are in Table 5.2. It is clear that the majority of the stars are K.

This result is significant for the NGTS project as it was hoped that a significant proportion of the stars that it would observe would be M-dwarfs to find smallest planets feasible from ground-based studies. That the majority of the objects are K instead with only a small sampling of M suggests that fewer M stars can be observed as the telescope can not achieve a sufficiently deep limiting magnitude to observe a large M population.

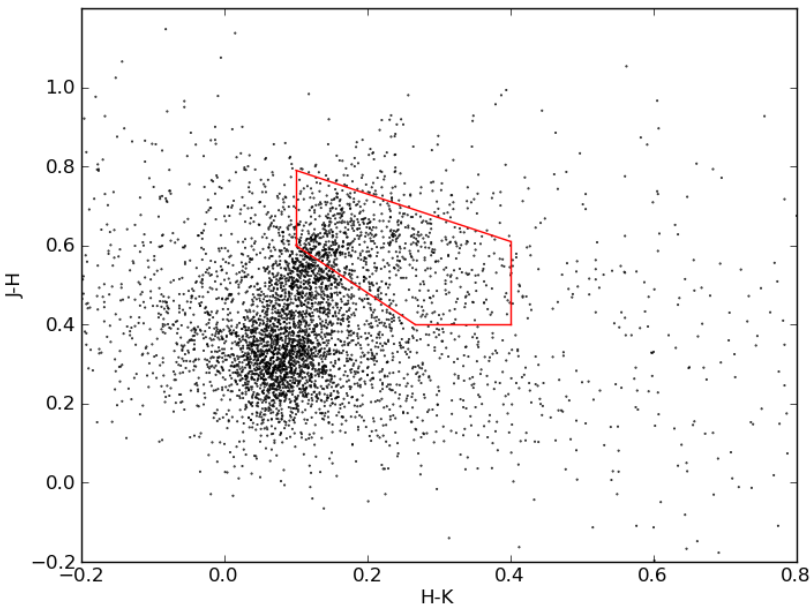

Figure 5.1: Colour cut defined in Equations 5.1 to 5.5, applied to Field 1, selecting M-dwarf candidates.

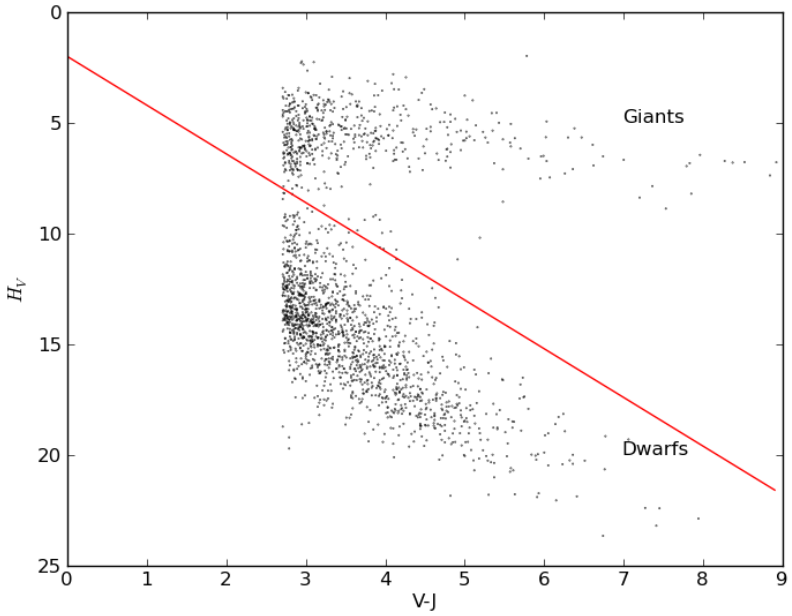

Figure 5.2: Reproduction of Figure 7 from Lépine and Gaidos, (2011). The red line is the cut from Equation 5.8. The colour axis has been extended for comparison with Figure 5.3.

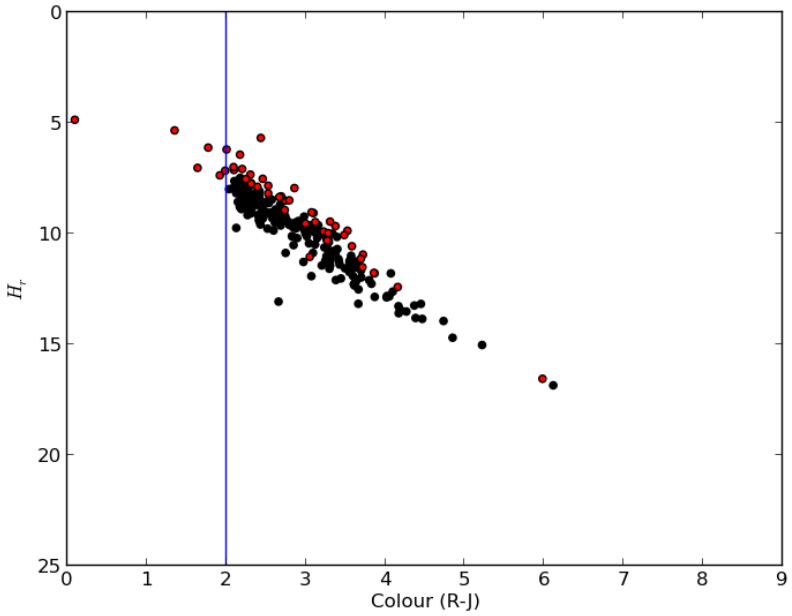

Figure 5.3: Colour reduced proper motion plot for stars from Figure 5.2 which have data in the Carlsberg Meridian Catalogue. Red objects are giants, black M dwarfs. The blue line is a cut generated by Equation 5.9.

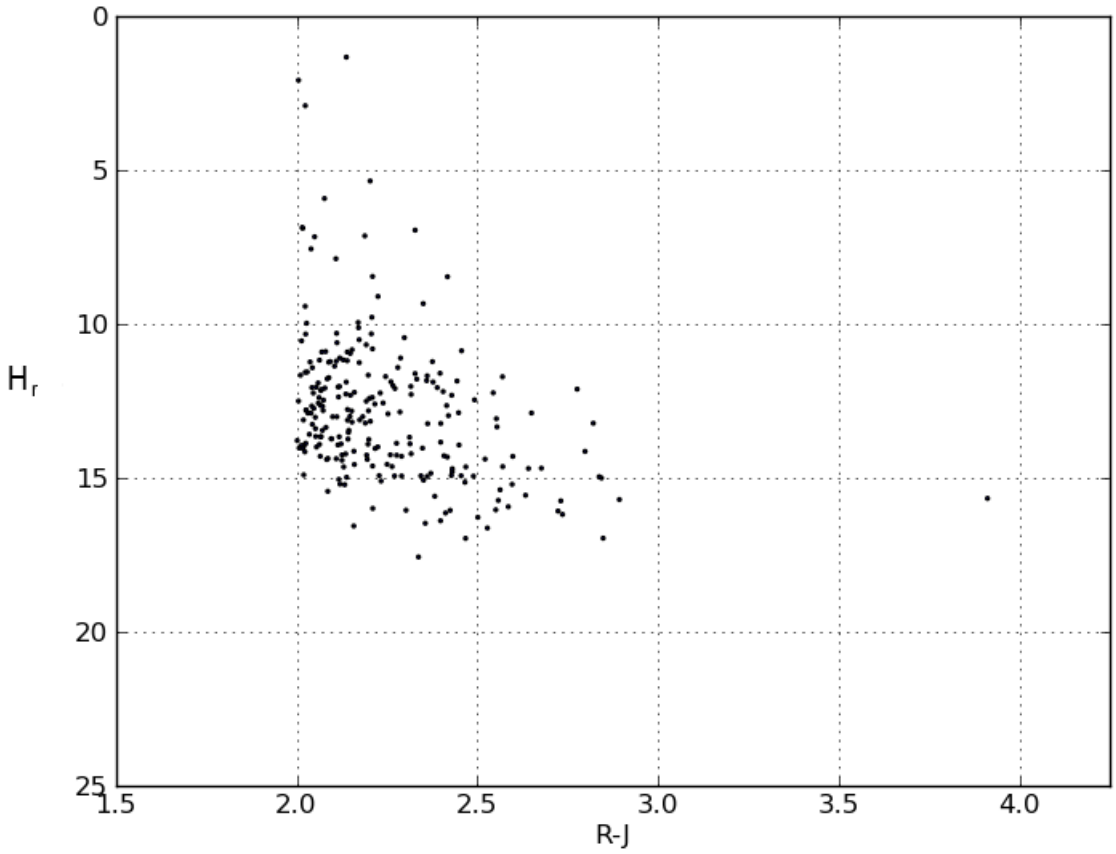

Figure 5.4: M dwarf candidates for the night 20091007. This is achieved using Equations 5.1 to 5.5 and 5.9. Comparison with Figure 5.2 suggests that the three stars with the lowest H_r are giants.

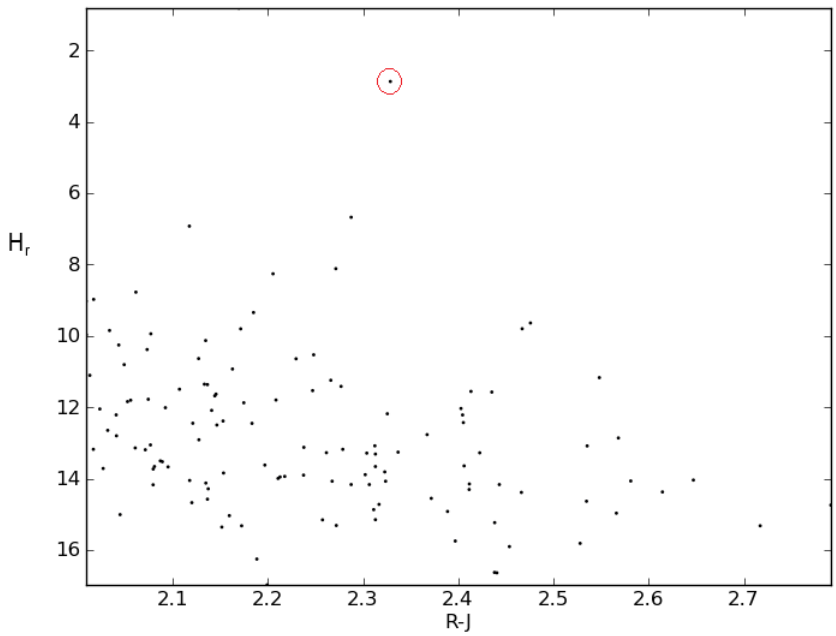

Figure 5.5: Reduced Proper Motion plot for field 1 M-dwarf candidates. One giant candidate might exist and is circled in red.

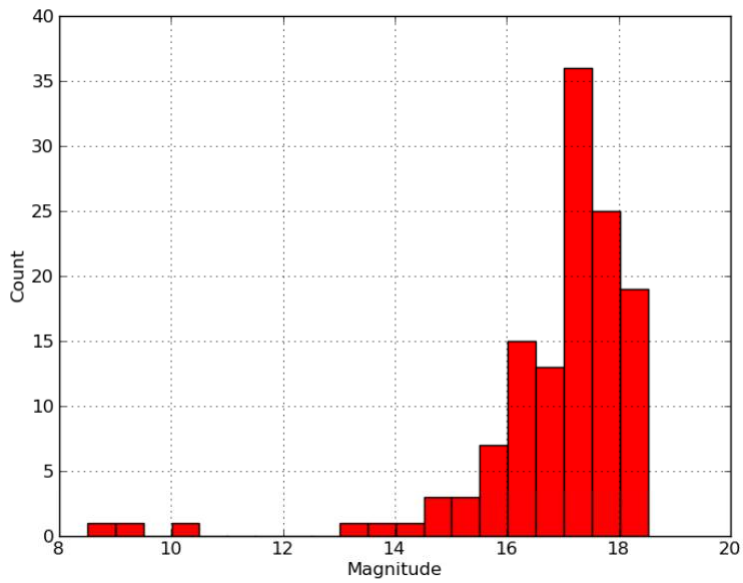

Figure 5.6: Magnitude distribution for the field 1 M dwarf candidates.

Chapter 6

Conclusions

The aim of this project was to characterise the stellar population observed by the NGTS prototype. The motivation for this is the ongoing hunt for extra solar planets and variable objects in our sky. The NGTS project is the next in a long, successful line of surveys operating towards this goal.

I began by introducing the NGTS prototype and the observations it had obtained. Thousands of images were taken during the final months of 2009 and the early months of 2010 at exposure times running from thirty seconds to three hundred seconds. Different focus settings were tested and observations were made of general fields, and specific events such as the WASP 11 transit. Certain nights, listed in Table 2.2, were selected for use during my project.

In Chapter 3 I covered the steps for astrometrically and photometrically calibrating the selected images. Three tools were tested for the astrometric calibration, with the aim of finding the most suitable one to be used in the data analysis pipeline for the NGTS project. All the tools exhibited strengths and weaknesses which will need to be considered before selecting the final method to be used.

SCAMP was found to be the most accurate tool but suffers from compatibility issues in regards to its use of header keywords. The requirement that an initial WCS solution exists for the images results in it also being the slowest of the three tools tested. WCS Tools was discovered to be the fastest, consistently obtaining a solution in less than five seconds per image. It, however, proved to be less accurate than SCAMP and requires specific image orientation to operate successfully. The final tool, Astrometry.net, was found to vary significantly in accuracy depending on image quality. Image quality was also found to impact speed of calibration, with solutions occurring within five to twenty seconds for defocused to focused images, respectively. It held the advantage that it could solve an image without any header

data.

Photometric calibration involved converting image magnitudes to a pseudo r band magnitude derived from the Carlsberg Meridian catalogue. Part of this process involved the construction of master images for the observed fields, obtained from stacking 25 individual images. It was found that the limiting magnitude could be increased to just beyond 18th mag in these stacked images. Finally a brief comparison was made between global and image by image photometric calibration, identifying that many nights were not perfectly photometric.

Chapter 4 followed on from Chapter 3 by generating light curves for all the identifiable objects within the calibrated images. These curves were then searched for variability using a χ^2 test. Systematic uncertainties associated with airmass were identified, and SYSREM was implemented to de-trend these effects. Significant improvement was observed by implementing a SYSREM correction to the light curves. Five variable objects were presented. One curve of good quality, with multiple observations over several nights was investigated with the aim of determining its period. The curve was tested under four different time series analysis methods and a period was identified at roughly 0.2 days, with the impression that the object was either an eclipsing binary or undergoing ellipsoidal modulation.

I also recovered the WASP 11 transit from the prototype data. After calibrating the light curve photometrically and detrending with SYSREM a transit depth of approximately 2% was determined. Comparison with a 2009 observation of the WASP 11 transit was undertaken. The transit depth and time from the NGTS prototype data matched that of the earlier observation which shows promise for the potential of the NGTS project.

Finally in Chapter 5 an in-depth investigation in to the spectral type distribution of the prototype fields was undertaken. Specific interest was taken in M-dwarfs due to the them being good candidates for finding small planets. A selection of colour cuts from a published study were taken to identify M dwarfs. In the NGTS prototype data an inability to find a suitable replacement for a cut made using V in the reference survey led to the final M dwarf candidate list likely containing some giant contamination. Some K-dwarf contamination was also confirmed.

No clearly variable objects were identified among the M-dwarf candidate list. Spectral classification was then extended to the rest of the objects in the fields. For the specific field tested, field 1 in Table 2.2, the majority of the objects, almost 80%, were identified as K stars. With only approximately 2% being identified as M dwarfs this would suggest that the limiting magnitude of NGTS is too shallow to observe large numbers of M-dwarfs, and that the search for smaller exo-planets will

have to focus on K-dwarfs.

Bibliography

AAVSO. American Association of Variable Star Observers. `http://www.aavso.org/`, 2011.

E. Bertin. Automatic Astrometric Calibration with SCAMP. In C. Gabriel, C. Arviset, D. Ponz, and S. Enrique, editors, *Astronomical Data Analysis Software and Systems XV*, volume 351 of *Astronomical Society of the Pacific Conference Series*, 2006.

E. Bertin and S. Arnouts. SExtractor: Software for source extraction. *Astronomy & Astrophysics Supplement*, 117:393–404, 1996.

E. Bertin et al. The TERAPIX pipeline. In D. A. Bohlender, D. Durand, and T. H. Handley, editors, *Astronomical Data Analysis Software and Systems XI*, volume 281 of *Astronomical Society of the Pacific Conference Series*, 2002.

L. Brát. Variable Star and Exoplanet Section of the Czech Astronomical Society. `http://var2.astro.cz/EN/tresca/transit-detail.php?id=1252467945`, 2009.

M. R. Calabretta and E. W. Greisen. Representations of Celestial Coordinates in FITS. *Astronomy & Astrophysics*, 395:1077–1122, 2002.

E. W. Greisen and M. R. Calabretta. Representaions of World Coordinates in FITS. *Astronomy & Astrophysics*, 395:1061–1075, 2002.

E. W. Greisen, M. R. Calabretta, F. G. Valdes, and S. L. Allen. Representations of spectral coordinates in FITS. *Astronomy & Astrophysics*, 446:747–771, 2006.

P. J. Groot et al. The Faint Sky Variability Survey - I. Goals and Data Reduction Process. *Monthly Notices of the Royal Astronomical Society*, 339:427–434, 2003.

J. D. Hartman et al. Deep MMT Transit Survey of the Open Cluster M37. II. Variable Stars. *The Astrophysical Journal*, 675:1254–1277, 2008.

R. Hill. Catalina Sky Survey. http://www.lpl.arizona.edu/css/index.html, 2003.

Institute for Astronomy University of Hawaii. Pan STARRS - Panoramic Survey Telescope Rapid Response System. http://pan-starrs.ifa.hawaii.edu/public/, 2005.

D. Lang, D. W. Hogg, K. Mierle, M. Blanton, and S. Roweis. Astrometry.net: Blind Astrometric Calibration of Arbitrary Astronomical Images. *The Astronomical Journal*, 139:1782–1800, 2010.

S. Lépine and E. Gaidos. An All-Sky Catalogue of Bright M Dwarfs. *The Astronomical Journal*, 142, 2011.

J. D. Mink. WCSTools 4.0: Building Astrometry and Catalogs into Pipelines. In *Astronomical Data Analysis Software and Systems XV*, 2005.

L. Morales-Rueda et al. Short time-scale variability in the Faint Sky Variability Survey. *Monthly Notices of the Royal Astronomical Society*, 371:1681–1692, 2006.

NASA. Kepler. http://kepler.nasa.gov/, 2012.

NGTS Partner Institutes. NGTS Next-Generation Transit Survey. http://www.ngtransits.org/index.shtml, 2012.

A. J. Norton. What is SuperWASP showing us? http://www.open.edu/openlearn/science-maths-technology/science/physics-and-astronomy/astronomy/what-superwasp-showing-us, 2012.

A. J. Norton et al. New periodic variable stars coincident with ROSAT sources discovered using superWASP. *Astronomy & Astrophysics*, 467:785–905, 2007.

A. J. Norton et al. Short period eclipsing binary candidates identified using superWASP. *Astronomy & Astrophysics*, 528, 2011.

A. J. Pickles. A Stellar Spectral Flux Library: 1150-25000 . *The Publications of the Astronomical Society of the Pacific*, 110:863–878, 1998.

D. L. Pollacco et al. The WASP project and the superWASP cameras. *The Publications of the Astronomical Society of the Pacific*, 118:1407–1418, 2006.

G. Ramsay and P. Hakala. RApid Temporal Survey (RATS) - I. Overview and first results. *Monthly Notices of the Royal Astronomical Society*, 360:314–321, 2005.

G. Ramsay, R. Napiwotzki, P. Hakala, and H. Lehto. RApid Temporal Survey (RATS) - II. Followup observations of four newly discovered short-period variables. *Monthly Notices of the Royal Astronomical Society*, 371:957–962, 2006.

J. D. Scargle. Studies in astronomical time series analysis. II - Statistical aspects of spectral analysis of unevenly spaced data. *Astrophysical Journal*, 263:835–853, 1982.

A. Schwarzenberg-Czerny. On the advantage of using analysis of variance for period search. *Monthly Notices of the Royal Astronomical Society*, 241:153–165, 1989.

A. Schwarzenberg-Czerny. Fast and Statistically Optimal Period Search in Uneven Sampled Observations. *Astrophysical Journal Letters*, 460, 1996.

D. L. Shupe et al. The SIP Convention for Representing Distortion in FITS Image Headers. In P. L. Shopbell, M. C. Britton, and R. Ebert, editors, *Astronomical Data Analysis Software and Systems XIV*, volume 30 of *Astonomical Society of the Pacific Conference Series*, 2005.

M. F. Skrutskie et al. The Two Micron All Sky Survey (2MASS). *The Astronomical Journal*, 131:1163–1183, 2006.

O. Tamuz, T. Mazeh, and S. Zucker. Correcting systematic effects in a large set of photometric light curves. *Monthly Notices of the Royal Astronomical Society*, 356:1466–1470, 2005.

M. B. Taylor. Stilts - A Package for Command-Line Processing of Tabular Data. In Daniel Ponz Carlos Gabriel, Christophe Arviset and Enrique Solano, editors, *Astronomical Data Analysis Software and Systems XV*, volume 351 of *Astonomical Society of the Pacific Conference Series*, 2006.

A. A. West et al. The Sloan Digital Sky Survey Data Release 7 Spectroscopic M Dwarf Catalog. I. Data. *The Astronomical Journal*, 141, 2011.

J. N. Winn. *EXOPLANETS*, chapter Transits and Occulations. University of Arizona Press, 2011.